2 CHAPTER II

LITERATURE REVIEW

Chapter II will be divide into three sections. The first section, brief histroy of *Candi Prambanan* is explained as an example to present general overview of common historical buildings exist in Indonesia. To add more, historical building that already experienced earthquake also will be explained. In the second section, preliminary numerical experiment using different method conducted by another author in the papers will be mentioned and discussed. The object of the historical buildings come in many shapes around the world. And in the third section, preliminary studied dicussing the influence of joint properties respect to masonry structure will be explained also.

2.1 History and Early Construction of *Candi Prambanan*

Indonesia is a home for thousands of temples. Temples in Indonesia already exist thousands of years ago. Temple is a symbol of ancient kingdom that once ruled in particular area. Among society, temple is also considered as sacred place. The particular reason for this circumstance is temple used to be place for the ceremony of a certain religion. In the present day, some of those temples already been excavated and studied, however there are still many of them have not been discovered yet. One of the biggest temples in Indonesia is *Candi Prambanan*, Figure 2.1

Candi Prambanan is a Hindu temple which already exist since 9th century in Klaten, Yogyakarta. *Candi Prambanan* was built during Sanjaya Dynasty reign

in Mataram Kingdom and considered as the biggest Hindu Temple in Indonesia. According to *Siwagrha* inscription, *Candi Prambanan* is dedicated to the *Trimurti,* the three essential gods in Hindu, which are Brahma (The creator God), Vishnu (The preserver God), and Shiva (The destroyer God). After *Mataram* Kingdom overthrown by an enemy, the *Candi Prambanan* was buried until it was discovered by C.A. Lons in 1733.

In the early of nineteenth century, *Candi Prambanan* was restored by the Dutch. Since that moment, *Candi Prambanan* undergo several restorations and become the object of interest for a lot of archaeologist and engineering, who are curious about the history and construction of the temple. In 1991, United Nations Educational, Scientific and Cultural Organization (UNESCO) listed the *Candi Prambanan* as a UNESCO World Heritage site no.642 in 1991 (Baba, 2007).

Figure 2.1 Candi Prambanan in Yogyakarta

Candi Prambanan does not refer to only a single temple structure, but Prambanan refers to the whole complex of the site. Prambanan complex is divided into 3 sections or zones where both those 3 zones are in the form of a square as depicted in Figure 2.2. The first section is the outer section that cover all the

Prambanan complex with dimension 390 m x 390 m wide. The second section is the middle section and cover an area with dimension 222 m x 222 m. In the second section, there are 224 *Candi Perwara* which arranged in 4 parts according to the 4 points of the compass-South, North, West, and East. And the last or third section is the main section or inner section with area dimension 110 m x 110 m. This last section is the most important and considered as the most sacred section of the Prambanan complex since the 3 main Trimurti Temple – Brahma, Vishnu, and Shiva, along with Wahana Temples and Apit Temples are located.

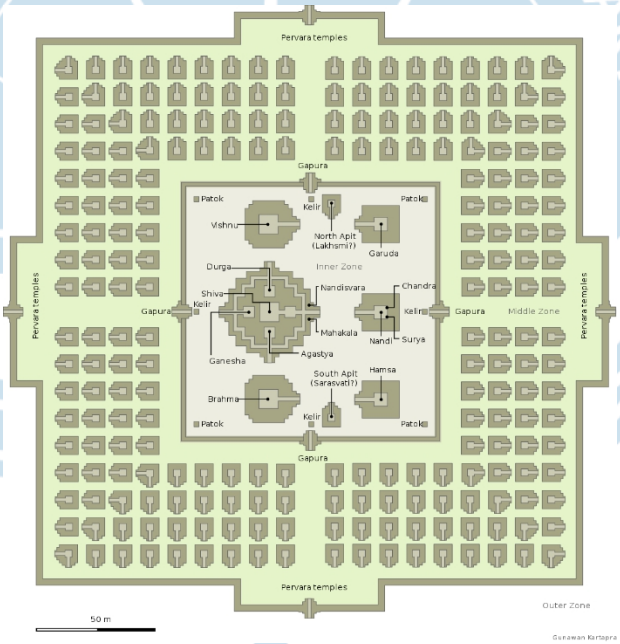

Figure 2.2 Candi Prambanan complex with 3 sections

Although in total there are 240 structures of the temples, in the present day, there are only 18 temples that stand still in the full structure. Except the main temples, the other temples' structures are only foundation that remains due to looting and natural disasters. The complete temple structures are depicted in Figure 2.3.

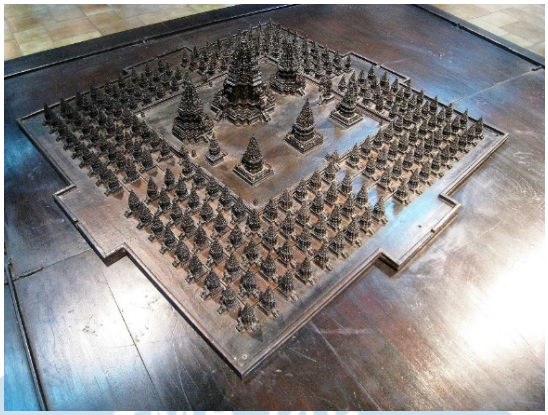

Figure 2.3 Mock up of complete Candi Prambanan

2.2 Numerical Method for Analysing Masonry Structure

The selected papers are the preliminary study that have been done by other authors. Each paper is discussed about the numerical analysis for a certain historical masonry structures which vary in shapes (wall, façade, bridge, and else). The methodology along with the assumptions in generating the geometry is mentioned and explained in detail. The Authors and papers discussing numerical method used for analysing the historical masonry structure are mentioned in Table 2.1. While the numerical method and numerical software used by the authors are mentioned in

Table 2.2 and Table 2.3, respectively.

Table 2.1 Authors and Papers Discussing Numerical Method Used for Analysing the Historical Masonry Structure

Number	Author	Paper
(1)	Thavalingam et al. (2001)	Computational Framework for Discontinuous Modelling of Masonry Arch Bridges
(2)	Giordano et al. (2002)	Modelling of Historical Masonry Structures: Comparison of Different Approaches Through A Case Study

(3)	Giamundo et al. (2014)	Evaluation of Different Computational Modelling Strategies for the Analysis of Low Strength Masonry Structures
(4)	Betti and Vignoli (2011)	Numerical Assessment of the Static and Seismic Behaviour of the Basilica of Santa Maria all'Impruneta (Italy)
(5)	Mendes et al. (2020)	Seismic Performance of Historical Buildings Based on Discrete Element Method (DEM): An Adobe Church
(6)	Kassotakis et al. (2020)	Three-dimensional Discrete Element Modelling of Rubble Masonry Structures from Dense Point Clouds
(7)	Perez-Aparicio et al. (2013)	Refined Element Discontinuous Numerical Analysis of Dry-Contact Masonry Arches
(8)	Hashimoto et al (2014)	Stability Analysis of Masonry Structure in Angkor Ruin Considering the Construction Quality of the Foundation
(9)	Kamai et al., (2005)	Dynamic Back Analysis of Structural Failures in Archeological Sites to Obtain Paleo-seismic Parameters using DDA.
(10)	Ma et al. (1996)	Seismic Analysis of Stone Arch Bridges Using Discontinuous Deformation Analysis

Table 2.2 Numerical Method Used by the Authors

Number	Author	FEM (Finite Element Method)	DEM (Distinct Element Method)	DDA (Discontinous Deformation Analysis)	Other Method
(1)	Thavalingam et al. (2001)	√	√	√	

(2)	Giordano et al. (2002)	√	√		√ (FEMDE)
(3)	Giamundo et al. (2014)	√	√		
(4)	Betti and Vignoli (2011)	√			
(5)	Mendes et al. (2020)		√		
(6)	Kassotakis et al. (2020)		√		
(7)	Perez-Aparicio et al. (2013)			√	
(8)	Hashimoto et al (2014)			√ (NMM-DDA)	
(9)	Kamai et al., (2005)			√	
(10)	Ma et al. (1996)			√	

Table 2.3 Software Used by the Authors

Number	Author	FEM (Finite Element Method)	DEM (Distinct Element Method)	DDA (Discontinous Deformation Analysis)	Other Method
(1)	Thavalingam et al.	DIANA	PFC (Particle Flow Code) 2D and 3D by	Shi's original DDA code	

	(2001)		Itasca, and 'FISH' language		
(2)	Giordano et al. (2002)	ABAQUS	UDEC by Itasca		Visual CASTEM 2000
(3)	Giamundo et al. (2014)	TNO DIANA v9.1	UDEC		
(4)	Betti and Vignoli (2011)	ANSYS v.11.0			
(5)	Mendes et al. (2020)		3DEC		
(6)	Kassotakis et al. (2020)		Self-develop software		
(7)	Perez-Aparicio et al. (2013)			Self-develop software	
(8)	Hashimoto et al (2014)			Self-develop software	
(9)	Kamai			Self-develop	

	et al., (2005)			software	
(10)	Ma et al. (1996)			Self-develop software	

Choosing suitable numerical method is a must procedure in analysing the masonry structure. The particular reason for this circumstance is each numerical method has its own assumption and different mechanism to carry out the analysis. Same object with the same parameter might has different analysis output when using different numerical method. There are two main basis of numerical method widely used especially in rock engineering field, those are based on continuity and discontinuity.

The famous example of the continuity is FEM (Finite Element Method) and example of the discontinuity are DEM (Distinct Element Method) and DDA (Discontinuous Deformation Analysis) (Nikolić et al., 2016). Basically, there are another numerical method which based on the discontinuity such as NMM (Numerical Manifold Method), FEMDE (Finite Element-Discrete Method), and else. Several papers mention in the

Table 2.2 are discussing those three main numerical methods along with the development and combination of other method. Furthermore, Table 2.3 is listed in detail related to the software that the authors use for running their analysis.

2.2.1 Numerical Method using Finite Element Method (FEM)

Finite Element Method or known as FEM is the basic numerical method that widely used for analysis in engineering field. FEM assumes that the object is linear and has continuous behaviour (Pérez-Aparicio et al., 2013; Thavalingam et al., 2001). Since the masonry structures are showing strongly non-linear and discontinuous behaviour, hence some improvement and certain assumptions are needed to be conducted in order to use this numerical method.

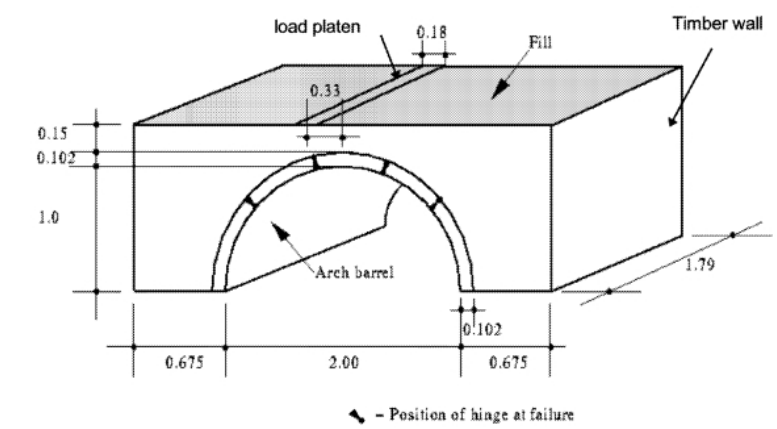

Figure 2.4 The profile of backfilled semi circular single span bridge (Thavalingam et al., 2001)

(Thavalingam et al., 2001) modelled the Bargower Bridge in England using non-linear finite element method. The profile of Bargower Bridge is depicted in Figure 2.4 with type of backfilled semi-circular single span bridge. Experimental test was conducted to validate the numerical result with the loading condition was located in the load platen as describe in Figure 2.4. The profile was built using grey class B bricks with ratio of cement: lime: sand as the mortar joints are 1:1:6, respectively. For the numerical test, the author using DIANA FE software and the geometry of the model is depicted in Figure 2.5.

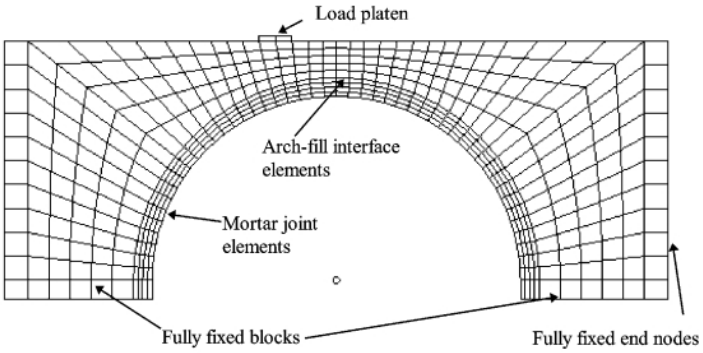

Figure 2.5 The geometry model of DIANA (Thavalingam et al., 2001)

The element shape used to simulate the highly various stress is by using four-node quadrilateral for the arch voussoirs and joints in the voussoirs were modelled with L8IF interface elements. While the interface between arch and the fill material was modelled by joint elements with zero thickness. The value for friction of the arch-fill interface was taken 75% of the fill friction, the cohesion was 0.03 and limited tension was 0.02N/mm2. Mohr-Coulomb criterion was adapted for the material properties of the interface. The loadings were assigned on the load platen with three points of loading.

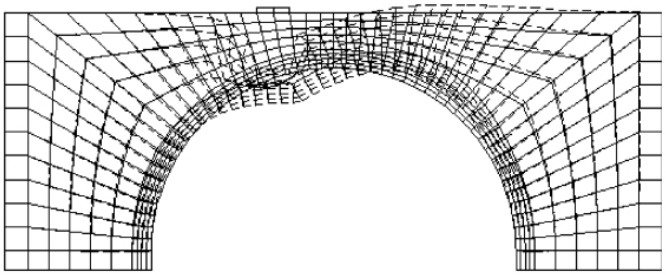

Figure 2.6 The deformation and failure mode of the arch bridge using FEM (Thavalingam et al., 2001)

Research by (Thavalingam et al., 2001) shows that numerical analysis using Finite Element Method (FEM) is capable to analyse the masonry structures,

but not fully accurate to predict the failure mode of the arch bridge. (Thavalingam et al., 2001) shows that using FEM, the predicted collapse load reach 128% of the experimental failure load which means it is higher than the experimental result that leads to un-accuracy of the result. The comparison of predicted collapse load between experimental and FEM is described in graph on Figure 2.7. While the deformation and failure modes of the arch model is depicted in Figure 2.6.

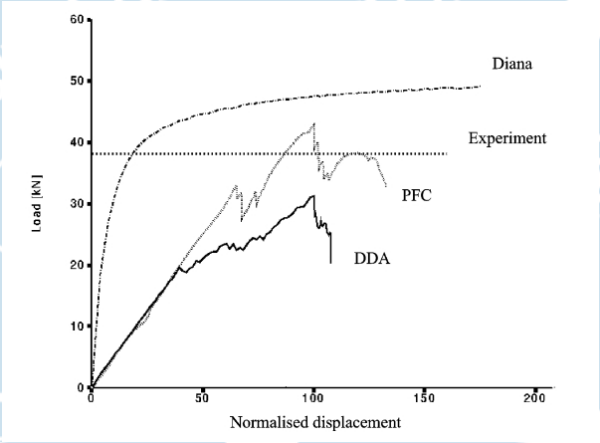

Figure 2.7 The comparison of the numerical and experimental result (Thavalingam et al., 2001)

(Giordano et al., 2002) in analysing the façade of the Sao Vicente de Fora monastery in Lisbon also admit that certain assumptions need to be conducted to generate and analyze the discontinuity of the masonry structure using FEM. Two model approaches can be used to model the discontinuity using FEM: the micromodel and macromodel.

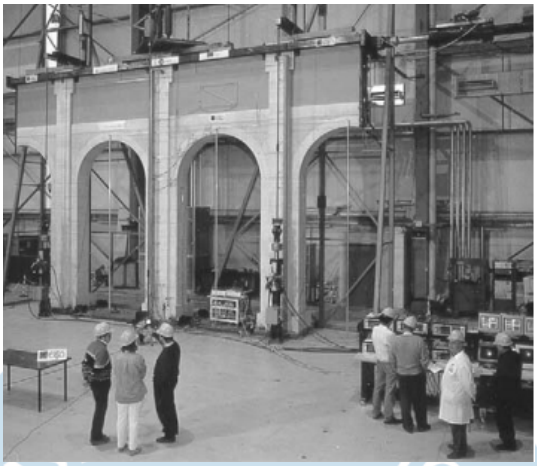

Figure 2.8 Profile of the façade (Giordano et al., 2002)

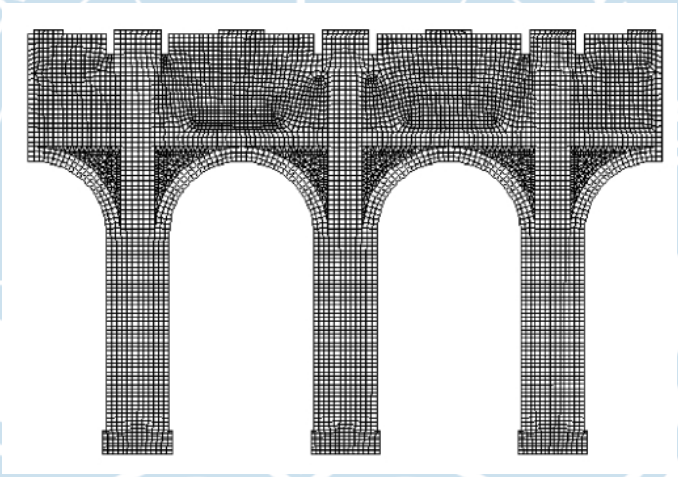

Figure 2.9 The façade modelled using ABAQUS (Giordano et al., 2002)

The profile of the façade covers three stone block column with two complete arches and two half arches. The detail profile is depicted in Figure 2.8, where it was used as the test model (experimental). The experimental result will be used to validate the result of the numerical test. ABAQUS was chosen to modelled and analysis the stresses of the façade. Homogenizated material and smeared cracking concept of constituve law were used for the analysis. Only the quasi-static test was perfomed, hence the push over curve could be compared with the monotonic experiment. The model using FEM is depicted in Figure 2.9 using

the S8R thick shell element (four-node quadrilateral), while the parameter value used for FEM is mentioned in *Table 2.4*.

Table 2.4 Parameter values for façade using FEM (ABAQUS) (Giordano et al., 2002)

	Stone	**Infill panels**
Weight per unit volume (kg/m3)	2500	2500
Young's modulus (Gpa)	65	6.5
Poisson's ratio	0.2	0.2
Compression strength (MPa)	30	7
Tensile strength (MPa)	3	0.7
***Failure ratios**	1.16, 0.1, 1.33, 0.28	1.12, 0.08, 1.33, 0.28

In the result of the numerical analysis, the assumption for the failure is assumed to be a simple Coulomb line and neglecting the reduction of the stiffness caused by inelastic straining, therefore this model is not able to predict the cyclic response since the cyclic behaviour is important in analysing the strength of masonry structure. Therefore, further investigations are needed.

Figure 2.10, which exhibit the graph of comparison between the experimental and numerical result can conclude two important subjects. The first one is the ultimate load from the numerical analysis is overestimated compare to experimental result. This might be caused by the different materials used for the experimental and numerical testing. The material infills and the arches are made from different materials which leads to different material properties. The particular reason for this circumstance is when the experimental test was conducted, the result shows sliding at the interface which is not allowed in the

finite element method, hence the material is substituted in order to avoid sliding at the interface for the finite element analysis.

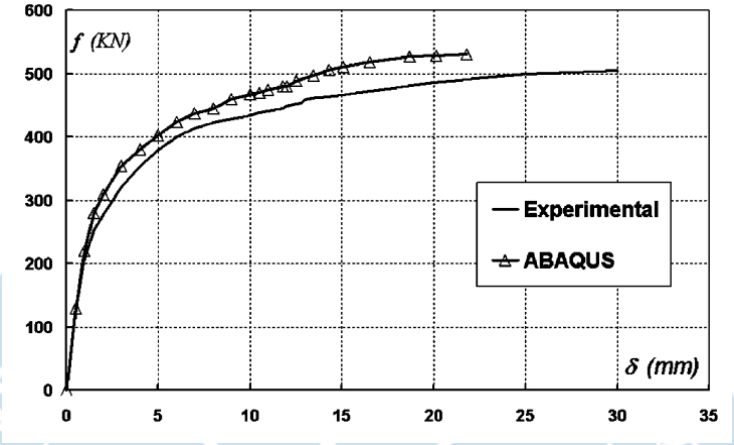

Figure 2.10 Comparison between experimental and numerical test (Giordano et al., 2002)

(Giordano et al., 2002) suggested to improve the computational effort to overcome the material gap although higher cost and choosing appropriate parameters may arise. The second issues are the curve looks stable that it should be probably because the experimental test was running not into collapse scheme, hence the cracking is limited.

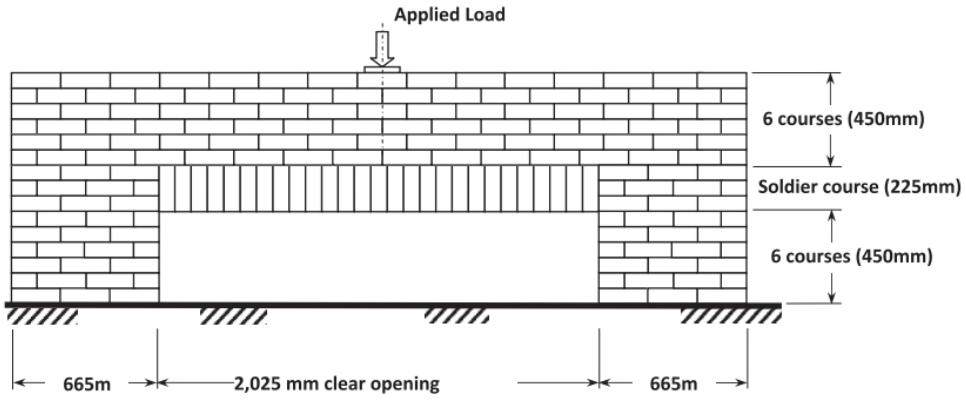

Figure 2.11 Profile of masonry wall (Giamundo et al., 2014)

To add more, (Giamundo et al., 2014) also using FEM to modelled a masonry wall and experiemntal test to validate the result with detailed profile is depicted in Figure 2.11.For the experimental test, (Giamundo et al., 2014) using four unreinforced masonry walls (S1, S2, S3, and S4) with bricks according to UK size that is 215mm x 102.5mm x 65mm. While the mortar joint thickness is 10mm and ratio 1:12 for opc : sand, respectively. The numerical analysis was performed using DIANA in 2D.

The element used for modelling the masonry wall was quadrilateral with four nodes, while the interaction between blocks and mortar joints was modelled using detailed micro-modelling as depicted in Figure 2.12. The discretization was based on the CQ16M eight-node quadrilateral isoparametric plane stress elements with meshing dimension 10mm for both bricks and mortar joints. (Giamundo et al., 2014) realized that the non-linear deformation of the bricks and local cracks are the main causes of the non-linear behaviour, hence those effects would be considered in the modelling of the masonry. Material properties that used in modelling the masonry is listed in

Table *2.5*.

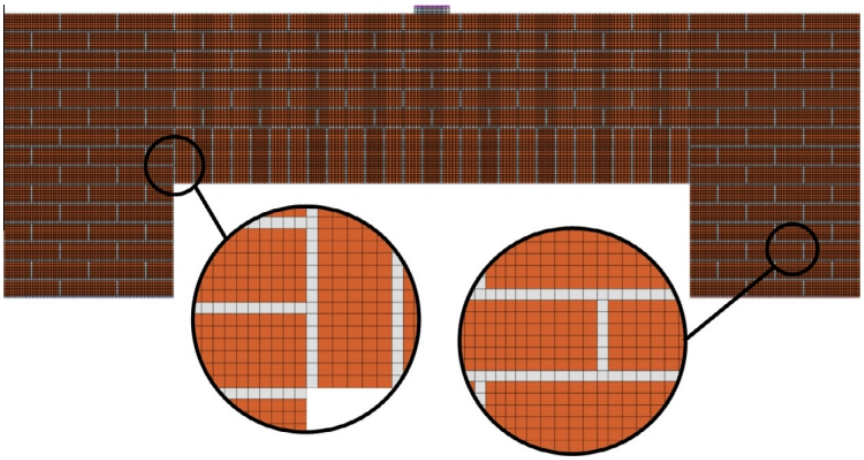

Figure 2.12 The geometry of the masonry wall using FEM (Giamundo et al., 2014)

Table 2.5 Material properties for model using FEM (Giamundo et al., 2014)

Material	E (Mpa)	fc (MPa)	ft (MPa)	Gc (MPa mm)	Gt (MPa mm)
Mortar	111.41	0.6	0.05	2.28E-01	1.59E-03
Bricks	1600	40	16	3.72E+00	5.98E-01

The comparison between the experimental and numerical test result is depicted on graph in Figure 2.13. On the graph in the Figure 2.13, both experimental and numerical result perform similarly same pattern up to displacement 0.5mm. On *Table 2.6*, it also mentioned in detailed the result of the experimental and numerical result for the first crack load and first crack deflection. Both experimental and numerical result also shows close and similarly same result for the deflection. But, for the displacement, the numerical test is terminated after reaching the peak displacement around 0.5mm.

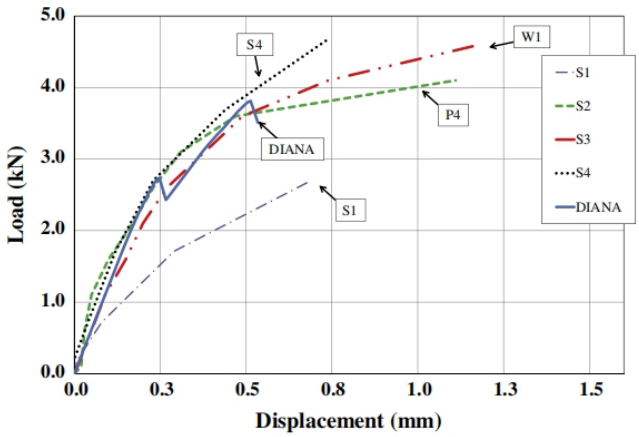

Figure 2.13 Comparison between experimental and numerical test using FEM (Giamundo et al., 2014)

The numerical test is not able to perform the post-peak behaviour of the masonry wall. (Giamundo et al., 2014) stated that the refined model of the finite element method could not fully capture the full displacement behaviour of the masonry structure. Large displacement may occurs in the masonry structure but it can not be analyse by the numerical test (FEM) since complete detachment is not allowed in FEM. Hence in Figure 2.13., the numerical result only able to perform the maximum displacement of the masonry wall before it fully detached.

Table 2.6 Experimental and numerical test result of masonry wall using DIANA (Giamundo et al., 2014)

Panel Name	First crack load (kN)	First crack deflection (kN)
S1	1.60	0.15
S2	1.60	0.10
S3	1.71	0.12
S4	0.72	0.08
FEM (DIANA)	1.52	0.12

(Betti & Vignoli, 2011) in their paper is using FEM to modelled and analyze the static behaviour and seismic vulnerability of the Basilica of Santa Maria all'Impruneta near Florence, Italy. They modelled the structure fully using FEM with dimension of the nave is 39.90m length, 14.50m width, and 15.0m for the wall height. While the thickness of the masonry wall is 0.70m for nave walls and 0.80m for the apse walls. Macro-modelling approach is chosen to modelled the geometry of the Basilica due to the non-linear behaviour of the structure. Homogenisated material along with smeared cracking and crushing constitutive law are take into account as the concept for analysing the Basilica.

The 3D approaches is perform to fully describe the behaviour of the Basilica. The model built using the code ANSYS v.11.0 where the masonry walls modelled with *Solid65* elements (three-dimensional eight noded isoparametric elements), for the main vault on the annexed buildings modelled with *Shell43* elements (isoparametric two-dimensional element with four nodal points), and last for the queen truss on the timber roof of the main nave modelled with *Beam44* elements (one-dimensional two noded isoparametric elements). Detailed geometry model is depicted in Figure 2.14.

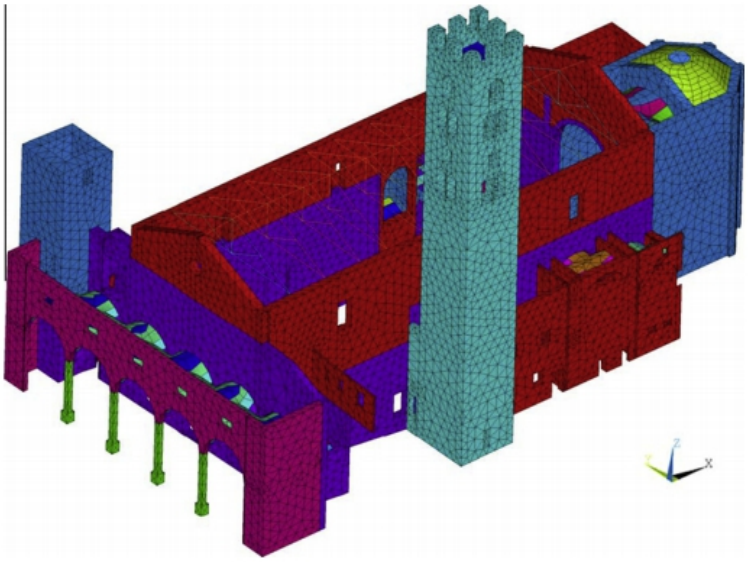

Figure 2.14 Geomertry of Basilica generated using Finite Element Method (Betti & Vignoli, 2011)

For modelling the whole structure of the basilica using FEM, the meshing consists of 27,779 nodes, 76,896 3D *Solid45* elements, 1751 2D *Shell63* elements, and 547 1D *Beam44* elements, that resemble to 81,021 degrees of freedom (Betti & Vignoli, 2011). While the elastic parameters are mentioned in detailed in Table 2.7. To perform the nonlinear behaviour, a Drucker-Prager (DP) perfectly plastic criterion is adopted for this model with detailed parameter is listed in Table 2.8. Another crtiterion used is William and Warnke (WW) failure surface criterion and the parameter is mentioned in Table 2.9.

Table 2.7 Elastic parameters of the Basilica modelled using FEM (Betti & Vignoli, 2011)

	Nave	Apse	Columns
Em (Young's modulus)	1400 N/mm^2	1530 N/mm^2	14,500 N/mm^2
V (Poisson's ratio)	0.2	0.2	0.2
Ym (Specific weight)	1900 kg/m^3	2000 kg/m^3	2300 kg/m^3

Table 2.8 Drucker-Prager yield criterion to perform the non-linear behaviour of the masonry structure (Betti & Vignoli, 2011)

	Nave	Apse	Columns
C (Cohesion)	0.1 N/mm^2	0.1 N/mm^2	0.5 N/mm^2
N (Flow angle)	15^0	15^0	15^0
0 (Friction angle)	38^0	38^0	38^0

Table 2.9 William and Warnke failure surface criterion of the masonry masonry structure (Betti & Vignoli, 2011)

	Nave	Apse	Columns
Fc (Uniaxial compressive strength)	7.5 N/mm^2	8.5 N/mm^2	40 N/mm^2
Ft (Uniaxial tensile strength)	0.15 N/mm^2	0.15 N/mm^2	3.5 N/mm^2
Bc (Shear transder coeff. Close crack)	0.75	0.75	0.75
Bt (Shear transder coeff. open crack)	0.15	0.15	0.15

The numerical analysis by (Betti & Vignoli, 2011) using non-linear FEM shows that the analysis was terminated when the horizontal loads reach up to 20% of the overall weight of the church. It also noted that the numerical analysis only able to perform the small displacement and cracking pattern as shown in Figure 2.15 and Figure 2.16, respectively. Hence, the total detachment was not perfomed

in this analysis. (Betti & Vignoli, 2011) also point out that since ANSYS was used to perform the analysis of the modal, any non-linearity was ignored. Figure 2.15 shows that the displacement mainly occur on the nave wall of the church in the transversal direction. Simultaneously, Figure 2.16 also shows the cracking pattern on the side wall and pronaos section in the transversal direction.

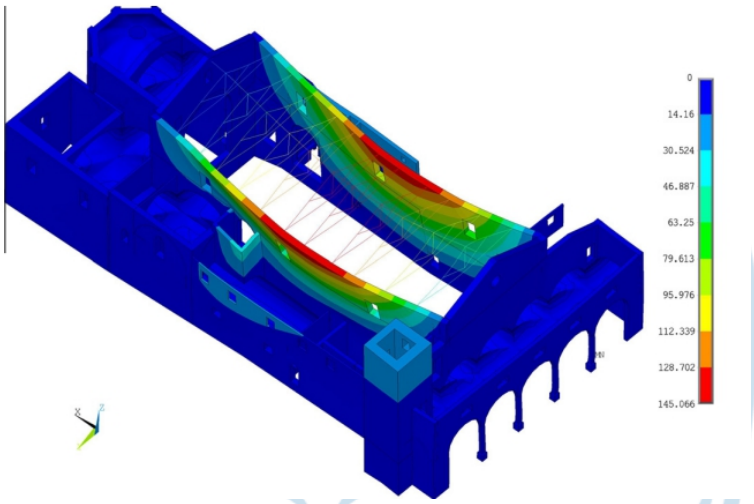

Figure 2.15 Displacement of the masonry structure (Betti & Vignoli, 2011)

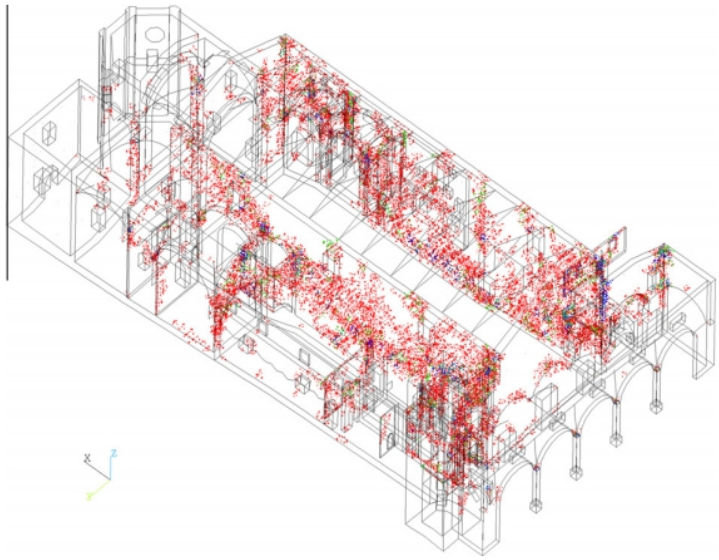

Figure 2.16 Cracking pattern of the masonry structure (Betti & Vignoli, 2011)

2.2.2 Numerical Method using Distinct Element Method (DEM)

The Distinct Element Method as a part of Discrete Element is another approach to be considered in modelling and analysing the behaviour of the masonry structure. Besides modelling the semi-circular single span bridge using FEM, as mentioned in section 3.1.1, (Thavalingam et al., 2001) also modelled the bridge using Distinct Element Method (DEM). The geometry of the span bridge is generate using Particle Flow Code (PFC) by Itasca. The geometry of the masonry generated by the PFC is shown in Figure 2.17. Using PFC, the author is able to model the masonry using spherical particles with single layer.

Modelling definition such as macros and algorithm such as 'FISH' languages is are used to modelled the backfill-arch and analyse the displacement. The masonry fill is modelled to become uniform therefore provisions for the mortar joint is not available. Each particle were placed and matched using its own coordinates and radius. While the voussoirs are modelled by joint plane option provided by PFC. Similar to FEM, the load is placed along the load platen on top of the masonry structure. By this modelling definitions, the backfill consists of 2175 particles while the voussoirs are divided into 24 division where each division consists of 16 fully bonded particles.

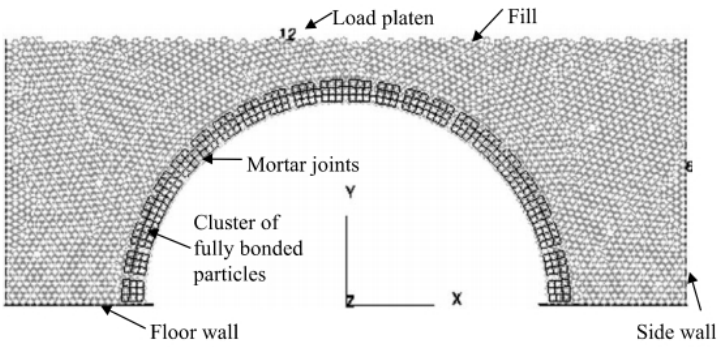

Figure 2.17 The geometry model using DEM (PFC) (Thavalingam et al., 2001)

The movement in each particles using DEM analysis is based on Newton Second law. The contact forces in normal and tangential directions is defined by the force displacement law. Later on, the other parameter such as accelerations, velocity and displacement are obtained by those contact forces. Each particle in DEM is assumed to be rigid but the contact is considered to be soft contact. In the computational procedure, the explicit time scheme is used to solve the dynamic equations. The contact between each particles are automatically update at a given time which caused the force updating also.

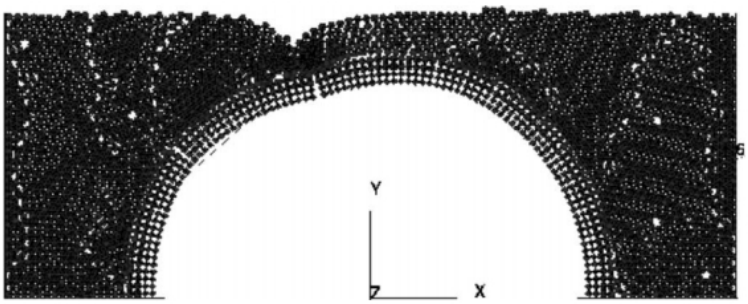

Figure 2.18 The deformation and failure mode of the arch bridge using DEM (Thavalingam et al., 2001)

In the numerical analysis using DEM by (Thavalingam et al., 2001), the simulation showed the preticted collapse load around 112% which is lower than result from FEM. The deformation only occur at the top of the fill masonry because the point load was assigned on the load platen at that location. The load only move vertically, hence the overlap stength of the structure can not be shown.

The joints at the arch show opening on the nearby location of the load. Since the blocks on the fill represent by a spherical element, when the load applied on the load platen, the adjecent element will attract the adjecent element. Unlike in the analysis using FEM where the elements were connected to each other, hence the elements attract simultaneously. The other section in the fill material was having small displacement due to displacement of the elements on the nearby of the load platen. The deformation and failure mode of the masonry using DEM is depicted in Figure 2.18.

(Giordano et al., 2002) also adopted another numerical method to analyse the masonry structure of Sao Vicente de Fora in Lisbon. (Giordano et al., 2002) stated that DEM (Distinct Element Method) is suitable for masonry structure which mostly the deformation occurs at joints or contact point. Each block in the masonry structure, which consists of several blocks, is assumed to be a single element that interacting one to another blocks through contact.

By using this assumption, (Giordano et al., 2002) could overcome two main difficulties when the author modelled the masonry structure using FEM. DEM could generate the geometry of the masonry simpler compare to FEM which

generating geometry of blocks and joints in FEM always become main problem. To add more, DEM provide remeshing methodology which allows update of the contacts between each block could be handled automatically.

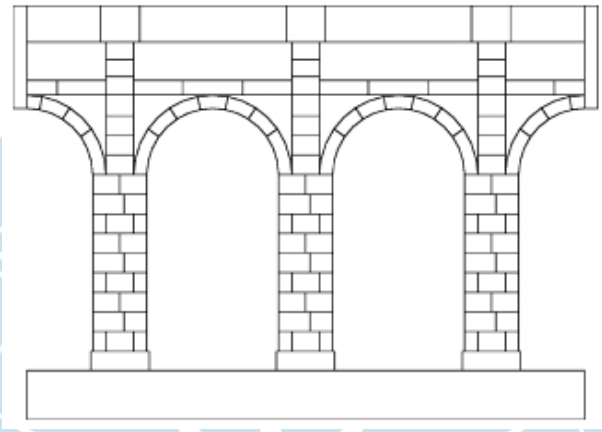

Figure 2.19 The geometry model using DEM (Giordano et al., 2002)

Since DEM employ explicit time logarithm, dynamic relaxation is used to perform the dynamic and quasi static analysis. In dynamic relaxation procedure, artificial viscous damping is necessary to apply in order to obtain the convergence or steady failure mechanism. The geometry of Sao Vicente de Fora generated using DEM is depicted in Figure 2.19. The analysis was conducted using computer software by Cundall which adopt the principle of DEM. This software namely UDEC (Universal Distinct Element Code) for two dimensional problems and 3DEC (3 Distinct Element Method) is available for three dimensional problems. The blocks in the model is assume to be deformable with material properties and parameters in UDEC mentioned in Table 2.10 and Table 2.11, respectively.

Table 2.10 Material properties of Sao Vicente de Fora (Giordano et al., 2002)

	Stones	**Infill panels**
Weight per unit volume (kg/m^3)	2500	2500
Young's modulus (Gpa)	65	6.5
Poisson's ratio	0.2	0.2
***kn*: normal stiffness (Gpa)**	115	-
***ks*: shear stiffness (Gpa)**	47.9	-
***Nt*: tensile strength**	0	-
***Ø*: friction angle**	30	-
***μ*: dilatancy angle**	5^0	-

Table 2.11 Parameter values in UDEC (Giordano et al., 2002)

	Value
***kn*: normal stiffness (Gpa)**	115
***ks*: shear stiffness (Gpa)**	46
***Nt*: tensile strength**	0
***Ø*: friction angle**	35
***μ*: dilatancy angle**	0
***c*: cohesion**	0

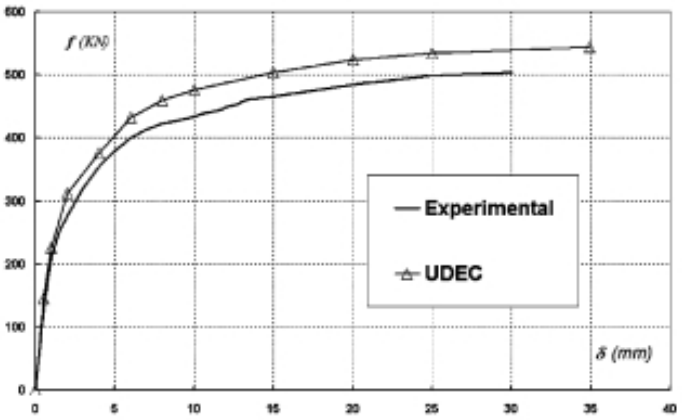

Figure 2.20 Comparison between experimental and DEM result (Giordano et al., 2002)

The comparison of the result using DEM and experimental test is perform in Figure 2.20. (Giordano et al., 2002) stated that tere are no limit for the

displacement when using DEM which become the advantages, however in the Figure 2.20, the analysis is stopped when the displacement reach 35 mm. The reason is just simply to compare the result of the displacement when using numerical and experimental test where the DEM can predict closest to the experimetnal result.

Using the same computer software, UDEC, (Giamundo et al., 2014) analyse the strength of masonry wall using DEM (Distinct Element Method). The geometry of the masonry wall was generated using DEM with following assumptions. The blocks on masonry wall was discretized, hence one block was depicted into one element. The blocks follow the common assumption in DEM, which assume the blocks to be deformable while the thickness of the mortar joints assume to be zero thickness. The detailed geometry of the masonry wall using DEM is depicted in Figure 2.21.

(Giamundo et al., 2014) also mentioned since DEM adopt the explicit time logarithm, this numerical method could solve the equations of motion promptly. To be more specific, the masonry wall only can be analyse using DEM if the numerical code allows finite displacements and rotations of each element until fully detachment. This is the paramount mechanism to generate important mechanism in discontinuous analysis, therefore if that mechanism cannot be fulfil, the discontinuous analysis cannot be satisfied. The other indicator that defines the DEM is recognizing new contact automatically. Since the element on DEM is not as much as in FEM, without the second indicator, the interaction of each distinct body will immediately recognized and lead to un-accuracy of the result.

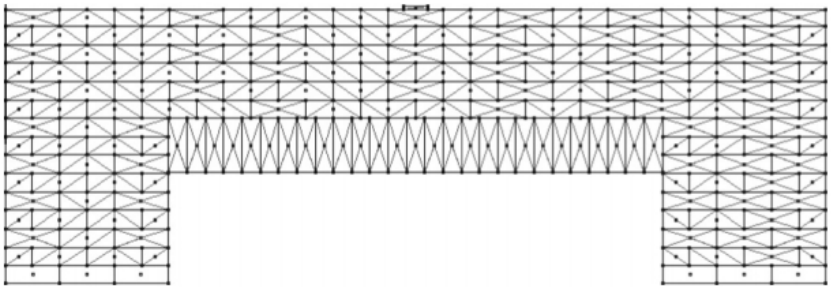

Figure 2.21 The geometry of the masonry wall using DEM (Giamundo et al., 2014)

Based on the common assumption where the mortar joints assume to have zero thickness, the geometry of the masonry wall was modified by the (Giamundo et al., 2014). In the real condition, the thickness of the mortar joints was 10 mm thick. Therefore, the size of each deformable block was increased up to 5 mm in every direction which resulting the size of each block become 225 x 112.5 x 75 mm using UDEC.

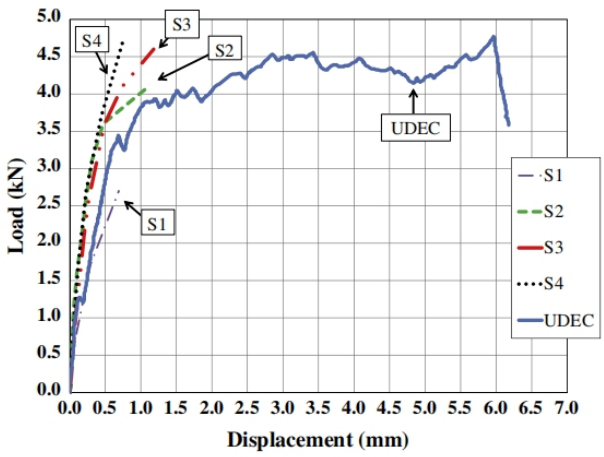

Figure 2.22 Comparison between experimental and numerical test using DEM (Giamundo et al., 2014)

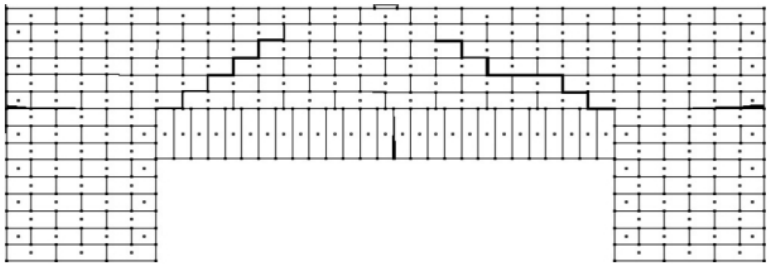

Figure 2.23 Failure locations predicted using DEM (Giamundo et al., 2014)

When the numerical test is conducted, the comparison between the experimental and numerical result is depicted in Figure 2.22. The S1 until S4 are obtained from the experimental result where its symbolized the panel ID. In Figure 2.22 when the load applied is 1.2 kN, the curve drops which the sign of the first crack in the masonry structure. While when the load applied around 4.75 kN, the curve drops drastically which indicates the masonry already fail or collapse. The locations of failure using DEM is depicted in Figure 2.23/

Further research using DEM was conducted by (Mendes et al., 2020). By using DEM, (Mendes et al., 2020) modelled Kuno Tambo Church in Peru to investigate the out of plane behaviour of the main façade in 3D under the earthquake exitacion. The condition of main façade of the church is depicted in Figure 2.24. The blocks of the church is made of adobe material or organic material which mostly made of earth, clay, straw, and else. This is the common material used for historical building in around seventeenth century. Adobe brick is manually shape and dry under the sun which made this material is durable, provide thermal and energy efficiency, sound insulation, and fireproof.

The geomtetry of the church is consist of façade and 10 m long of longitudinal wall. the software used to generate the geometry of the façade is 3DEC software (the 2D version is UDEC) by Itasca. The geometry of the main façade and longitudinal wall in 3D is depicted in Figure 2.25. The structure is divided into two sections, the adobe blocks and the base which made of stone. For both sections, the blocks are assumed as rigid blocks. Voronoi polygons is choosen to model the base section of the masonry with upsizing the dimension of the stone blocks. Therefore the computational effort can be reduce since the geometry of the adobe block generated using DEM consist of around 6,886 blocks.

Figure 2.24 Main Façade of Kuno Tambo Church in Peru (Mendes et al., 2020).

The density of the stone and adobe blocks is 19 kN/m^3, where the value is obtained correponds to the density of the masonry and considering the modelling approach (Mendes et al., 2020). While the value of the interfaces properties are mentioned in Table 2.12. (Mendes et al., 2020) on this research sets three hypotheses (model) for the connection between the main façade and the longitudinal walls. In the first model, the joint is assumed to be inelastic with

material properties of the adobe are tensile strength (f_t) equal to 0.12 MPa, friction angle (Ø) equal to 29^0 and cohesion (c) equal to 0.18 MPa (Mendes et al., 2020). On the other hand, joint at the second model is assumed to be elastic with stiffness value equal to mud mortar. And for the last model, the joint is assumed to have very week connection where the material properties of the mortar are (f_t) equal to 0.01 MPa, friction angle (Ø) equal to 29^0 and cohesion (c) equal to 0.044 MPa (Mendes et al., 2020).

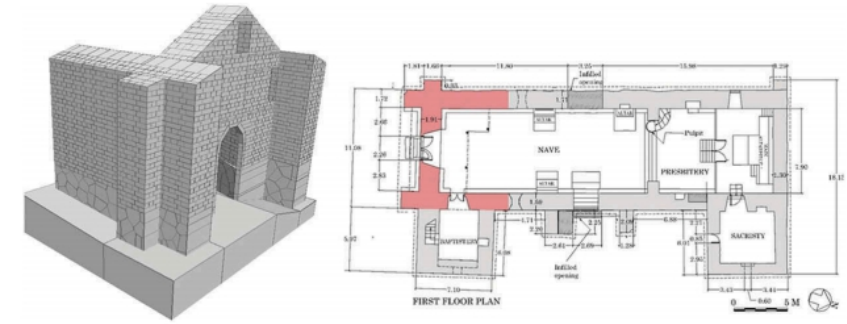

Figure 2.25 Geometry of the façade and longitudinal wall in 3D (Mendes et al., 2020)

For the earthquake exitaciton, the dynamic tests are conducted to estimate the modes applied on the masonry structure. From the dynamic tests, four modes are obtained with frequency raning from 1.59 Hz to 2.99 Hz (Mendes et al., 2020).

Afterwards, the pushover analysis is conducted to evaluate the performance of the main façade and the longitudinal wall under seismic response. The analysis covers the orthogonal direction, inward (+Y) and outward (-Y) of the main façade. The result of the analysis shows the collapse mechanism of the façade for inward (+Y) and outward (-Y) in Figure 2.26(a) and Figure 2.26(b),

respectively. For outward direction (-Y), the maximum horizontal acceleration is 0.24 g for Model 1, 0.34 g for Model 2, and 0.15 for Model 3. For all models, mostly the failure mechanism or the cracks started at the connection between the the main façade and the longitudinal wall. While for the inward direction (+Y), the capacity of horizontal acceleration shows relatively small compare to outward direction (-Y). The horizontal accelerations are 0.19 g, 0.37 g, and 0.14 g for Model 1, 2, 3, respectively. The failure mechanism almost the same with the outward direction, where the initial cracks due to overturning occur at the connection of the main façade and the longitudinal wall. However, Model 2 shows peculiar failure mechanism where the longitudinal wall is collapse and has complete detachment.

Table 2.12 Interfaces properties of the masonry (Mendes et al., 2020)

	Stone-Stone Interface	**Adobe-Adobe Interface**	**Adobe-Stone Interface**
Cohesion: c (MPa)	0.100	0.044	0.065
Firction angle: Ø (^{0})	22	29	24
Tensile strength: f_t	0.050	0.010	0.010
Normal stiffness: K_n (GPa/m)	1.04	0.40	0.62
Shear stiffness: K_s (GPa/m)	0.42	0.16	0.25

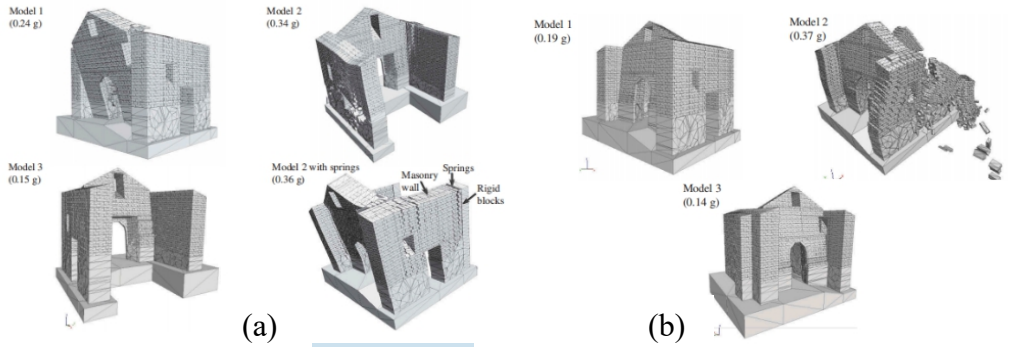

Figure 2.26 Result of pushover analysis in: (a) outwards (-Y) and (b) inwards (+Y) (Mendes et al., 2020)

The last research about DEM was conducted by (Kassotakis et al., 2020). The object of the research is Caerphilly Tower in South Wales, UK, as seen in Figure 2.27 which already exist since 13th century and become the second largest tower in Europe. In the Figure 2.27 can be seen that the southwest tower in leaning and the research was aiming to evaluate the proposed framework of the tower (Kassotakis et al., 2020). The diameter of the tower is 9 m and the height is 17 m tall, while the approximate inclination is 10^0 vertical. In this research. (Kassotakis et al., 2020) using dense point cloud to caoture the whole geometry of the structure, then using Matlab, the point clouds were executed to obtain the coordinate, therefore the geometry of the blocks can be discretized using DEM. For the DEM analysis, the geometry of the tower is generated using 3DEC for 3D problem.

Figure 2.27 Caerphilly Tower in South Wales, UK (Kassotakis et al., 2020)

The structure of the tower in DEM is modelled using discrete blocks separated by zero thickness mortar joints. The element of the blocks is voxels (8 noded polyhedron) since some part of the tower already destroy (rubble). The blocks are assumed to be rigid blocks with density equal to 1,900 kg/m^3 (Kassotakis et al., 2020). While the value of other mechanical properties are listed in

Table 2.13. The geometry of the tower generated using 3DEC is depicted in Figure 2.28, where the gold area is the original geometry of the tower and the green area is the additonal base for the tower.

Table 2.13 Joint properties of the tower (Kassotakis et al., 2020)

	Value
Joint Normal Stiffness: Kn (GPa/m)	20
Joint Shear Stiffness: Ks (GPa/m)	15
Joint Cohesion: c (MPa)	0.25
Joint Tensile Strength: T (MPa)	0.25
Joint Friction Angle: Ø (^{0})	25

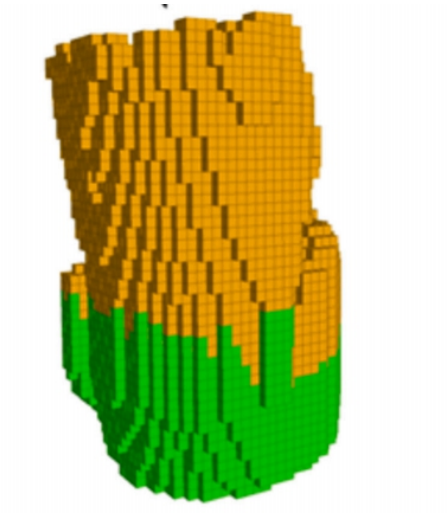

Figure 2.28 Geometry of the tower using DEM (Kassotakis et al., 2020).

The proposed framework is to investigate the influence of the block size respect to displacement of the blocks in the masonry. The size of the voxels are determined for 50 cm, 40 cm and 30 cm. The geometry of the different voxels are depicted in Figure 2.29 with inclination 60^0. For voxel with size of 50 cm, the total blocks generated is 13,385 with total contacts 155,556. When the size of the voxel become finer equal to 40 cm, the total blocks generated is 22,532 with total contacts 155,556. The number of the blocks generated by voxel's size of 30 cm is 47,827 with total contacts 576,449. The monitoring points for evaluating the behaviour of the blocks are located in three point; top, mid-height, and base, respectively.

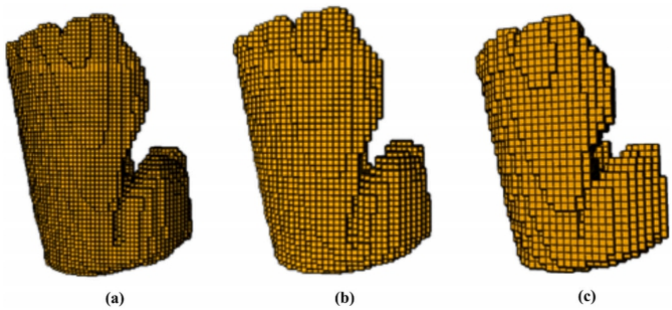

Figure 2.29 Geometry of the tower using different size of voxels: (a) 30 cm, (b) 40 cm, and (c) 50 cm (Kassotakis et al., 2020)

The results obtained from the analysis are listed in *Table 2.14*, which shows that the decrease of the voxel's size resulting on the decrease of the displacement in three points of observation. (Kassotakis et al., 2020) stated that the block size has important role in determining the capacity of the structure because the joints form planes of weakness in the structure. The failure mode from each different voxel's size are depicted in Figure 2.30. To conclude, (Kassotakis et al., 2020) also stated that DEM shows good performance in capturing the collapse and post-collapse behaviour accurately although detail geometry and information about the masonry structure are needed.

Table 2.14 Displacement's result respect to the voxel's size (Kassotakis et al., 2020)

Size (cm)	λh, max	Uh (A), max (mm)	Uh (B), max (mm)	Uh (C), max (mm)
50	0.18	6	3.8	1.8
40	0.14	5.6	3.0	1.4
30	0.06	2.0	1.0	0.3

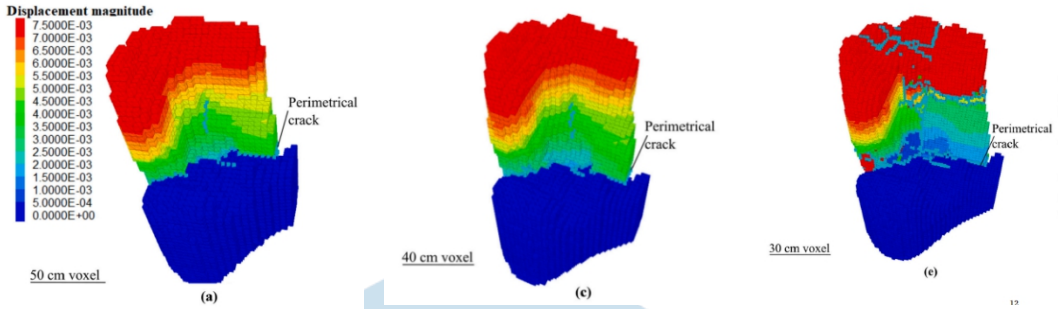

Figure 2.30 Failure mode of the tower using DEM (Kassotakis et al., 2020).

2.2.3 Numerical Method using DDA

Besides modelling using non-linier finite element and distinct element method, (Thavalingam et al., 2001) also modelled the backfilled masonry arch bridges as a comparison to another numerical method. The basis of the DDA (Discontinous Deformation Analysis) similar to DEM (Distinct Element Method) which emphasize on the discrete system of each element. The discritize blocks were analyze by the fundamental principle of the discontinuity analysis. DDA method, which developed by Shi, basically develop for analysing problems in rock engineering. The static and dynamic loading assigned on the blocks can be solve simultaneously using this method. Contrasting with the DEM, the blocks in DDA are assumed to be deformable or elastic, while the contacts bwtween each block are considered as hard/rigid contact (Thavalingam et al., 2001).

The backfilled masonry arch bridge is modelled into semi circular arch which then the geometry was generated using DDA as depicted in Figure 2.31. The dimension of the arch also mentioned in detail in Figure 2.31 and the dimension was referring to the real dimension of the bridge itself. The fill of the bridge was modelled using polygonal shape element since there are no provision

for the shape of the element, hence the shape can be arbitary. Using DDA, the fill of the masonry was modelled using 750 DDA elements. While for the arch, it was modelled with square elements connected with mortar joints. The value for friction of the arch was taken as 75% of the friction of the fill material (Thavalingam et al., 2001).

The side wall was modelled fully fixed at the centroid in order to simulate the deformability of the sidewall. While the bottom blocks were setted fully fixed. The load was placed on the load platen where the algorithm of displacement derives from the load already developed in order to capture the collapse response and mechanism of the blocks. Unlike FEM or DEM, DDA does not have commercial and official software, hence (Thavalingam et al., 2001) uses self develop software which based on Shi's original DDA code.

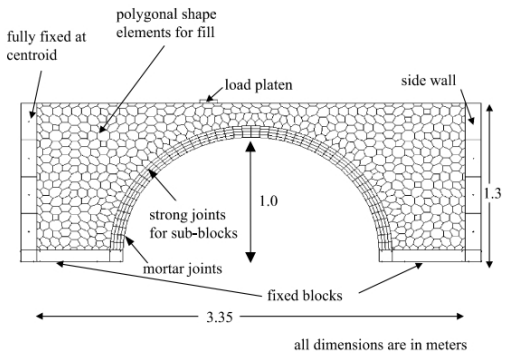

Figure 2.31 The geometry of backfilled masonry arch bridges using DDA (Thavalingam et al., 2001)

Comparing to numerical analysis using FEM and DEM by (Thavalingam et al., 2001), DDA shows best performance among the other method. From the numerical simulation, it was found that DDA model can predict a lower collapse

scenario with percentage about 84% of the result from the experimental test. (Thavalingam et al., 2001) stated that DDA shows fewer convergence problem comapre to FEM. The iteration procedure using DDA was terminated when the post-peak response was satisfied due to non-convergence in the algorithm. Since the framework of DDA is adopting the concept of constanct stress for each block, it result to the strong connection of the joints for the arch.

Therefore, the deformation due to load on the load platen did not generate displacement in the arch section. The deformation and failure mode of the bridge using DDA is depicted in Figure 2.32. (Thavalingam et al., 2001) conclude that sensitivity analysis should be conducted to exhibit the imporatance of the material and joint properties respect to the collapse scenario of the masonry structure. To add more, analysis using earthquake load also need to be perform since the current research only assign a point load on a certain section. This cannot truly decribe the overall strength of the masonry structure.

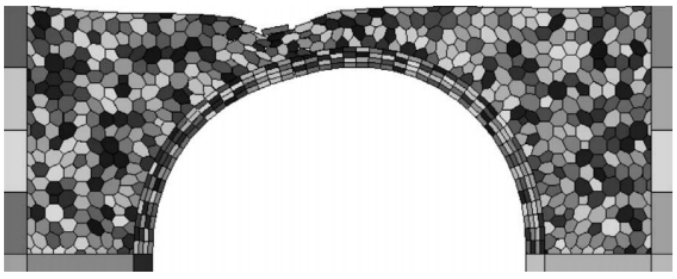

Figure 2.32 The deformation and failure mode of the arch bridge using DDA (Thavalingam et al., 2001)

(Pérez-Aparicio et al., 2013) using DDA was analyzed the burried arch or vault under vertical loading and terrain filling. Unlike previous reseach by

(Thavalingam et al., 2001), where the load is subjected to load platen on the top of the filling, in the research by (Pérez-Aparicio et al., 2013), the load is subjected along the arch. The arch was burried in the soil, hence the soil become the load subjected into the arch. The dimension and load subjected into the arch is decribe in Figure 2.33.

The arch were modelled into discrete dry blocks where the curvature of the arch produce the stability of the arch. The roughness of the blocks also define the contact and friction of each block. The foundation of the arch is assume to be fixed or rigid to prevent from moving mechanism, which is essensial for the boundary condition. (Pérez-Aparicio et al., 2013) particularly simulate the collapse mechanism generated by the instability of the arch. Material properties of the blocks were assume. Young's modulus (E) of each block is chosen to be high enough as 1 x 10^9 to indicate the high stiffness of the blocks. The other material properties were summarized in Table 2.15.

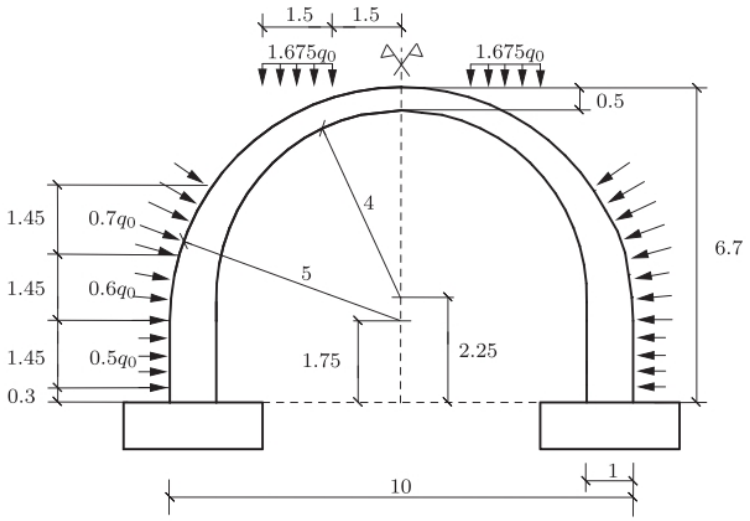

Figure 2.33 Dimension and load subjected into the arch or vault (Pérez-Aparicio et al., 2013)

Table 2.15 Material properties of the blocks (Pérez-Aparicio et al., 2013)

Property	Value	Units
Stone Young's modulus, E	1 x 10^9	N/m^2
Stone Poisson's coeff.	0.25	-
Stone density	2300	Kg/m^3
Stone strength (compr)	1 x 10^7	N/m^2
Stone friction	30^0	
Stone cohesion	0	N/m^2
Filling density	1600	Kg/m^3
Filling friction	30^0	

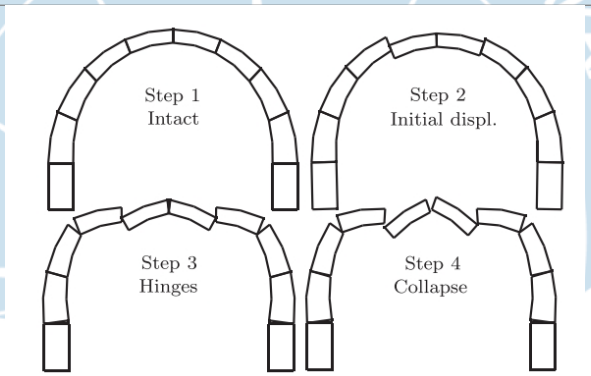

Figure 2.34 Sequence of collapse for arch with 9 joints (Pérez-Aparicio et al., 2013)

In the analysis using DDA, there are 4 steps in capturing the collapse mechanism of the arch. The q_0 as the external load is remain unknown to reach the collapse mechanism, hence the author assume to set the external load starting from 5 kN and increasing until the collapse mechanism is satisfied. At the 2nd step when the initial displacement is reached, the external load is kept constant until collapse happened. The arch is modelled with different number of joint. Four analysis are run for arch with 9, 17, 27, and 61 joints. From the analysis it was found that arch with different number of joints has different collapse mechanism.

The sequence of the collapsing mechanism of each arch with 9, 17, 27, and 61 joints is depicted in Figure 2.34, Figure 2.35, and Figure 2.36 respectively.

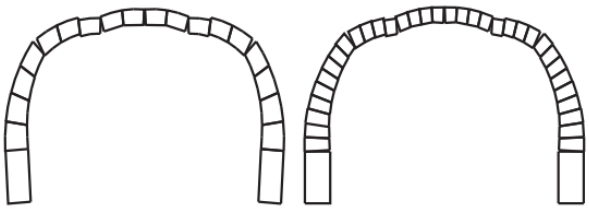

Figure 2.35 2nd step of collapsing (initial failure) for arch with 17 and 27 joints (Pérez-Aparicio et al., 2013)

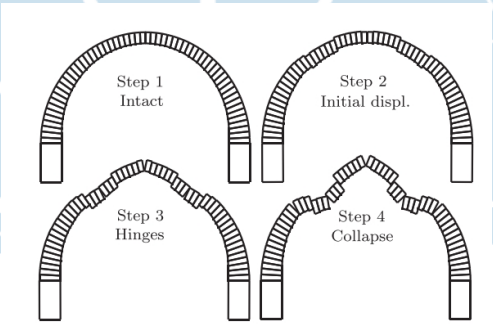

Figure 2.36 Sequence of collapse for arch with 61 joints (Pérez-Aparicio et al., 2013)

The comaprison of the experimental and numerical result result of the load applied into the arch with different number of joints are described in Table 2.16. The higher the number of joint, the load causing the arch to collapse is smaller. (Pérez-Aparicio et al., 2013) stated that this is the consequence of having more joints in the arch. When more joints applied in the arch, accordingly more weak points in the arch are exist hence the sliding or turning highly to happen. In Table 2.16 can be seen also that the error decrease as the decreasing number of the joints.

According to (Pérez-Aparicio et al., 2013), solution in DDA become better when higher number of element is applied because the analysis is less sensitive towards the uncertainties.

Table 2.16 Experimental and Numerical result of q0 applies until collapse (Pérez-Aparicio et al., 2013)

# Joints	Critical Load Experiment	Critical load DDA	Error %
9	250	280	12.2
17	206	210	1.6
27	206	205	-0.8
61	205	205	0.1

Another research analysing the masonry structure using DDA (Discontinous Deformation Analysis) was conducted by (Hashimoto et al., 2014). The object of the research is Angkor Ruin in Cambodia which become the World Culture Heritage. The research was conducted to analyse the stability of the Angkor masonry structure due to comapaction of the rammed soil beneath the structure. Uneven settlement of the soil or the rammed earth cause decline of the upper structure. This event cause joint openings of the structure and inclination approximately up to 4.6% (Hashimoto et al., 2014). Prasat Suor Prat N1 Tower was choosen to become the object of the study to represented the stability of Angkor Ruin.

The numerical simualtion was conducted using combination of DDA and NMM (Numerical Manifold Method). The masonry blocks of the tower were modelled using DDA, while the rammed earth was modelled using NMM. The masonry blocks were assumed as linear elastic, while for the foundation, the

modified cam-clay was adopted (Hashimoto et al., 2014). The geometry of the masonry structure with the foundation generated by DDA-NMM as well as the dimension is depicted in Figure 2.37. While the material and joint properties of the masonry blocks are listed in detail in Table 2.17 and Table 2.18, respectively. The critical state stress ratio (M) of the natural ground was obtained from the laboratoty test, therfore the internal friction angle (Ø) was assumed to be 30^0 (Hashimoto et al., 2014).

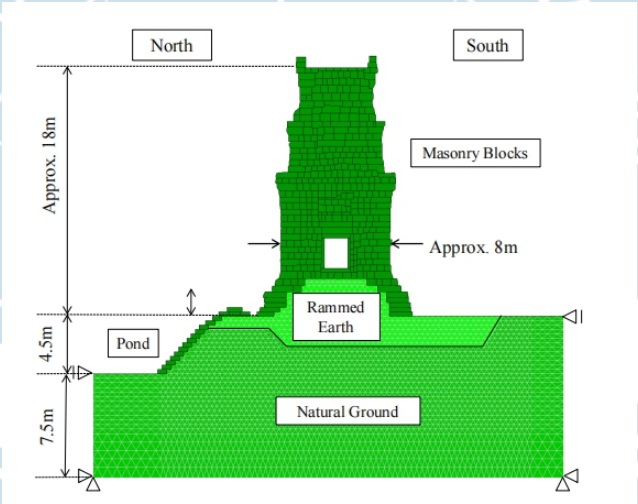

Figure 2.37 Geomertry of the Angkor Ruin generated by DDA (Hashimoto et al., 2014)

Table 2.17 Material properties for the Angkor Wat (Hashimoto et al., 2014)

	Masonry block	**Rammed Earth**	**Natural ground**
Constitutive model	Linear elastic	Subloading modified Cam-clay	
Unit weight: [kN/m^3]	30	18	18
Elastic modulus: [kPa]	1x10^6	-	-
Compression index:	-	0.0580	0.0782
Swelling index	-	0.00484	0.00711
Poisson ratio	0.2	0.3	0.3
Critical state stress ratio: M	-	1.37	1.2
Void ratio on normal	-	0.700	0.478

consolidation line at p=98 [kPa]:			
Parameter of subloading surface: a	-	25	100

Table 2.18 Joint properties for the Angkor Wat (Hashimoto et al., 2014)

	Value
Normal direction penalty stiffness [kN/m]	5.0×10^5
Shear direction penalty stiffness [kN/m]	5.0×10^3
Surface friction angle [^{0}]	36
Open-Close criterion	1.0×10^{-5}
Close-Open criterion	1.0×10^{-8}
Assumed maximum displacement ratio	0.001

To further investigation on the comapction of the rammed earth, two cases were setted. The Case A with the value of initial void raio of the rammed earth is 0.399 where the rammed earth was compacted with optimum water content, on the other hand, the Case B adopted loosen comapaction with the value of initial void raio of the rammed earth is 0.500 (Hashimoto et al., 2014). The result of the analysis showed that the treatment on Case A and Case B resulting on the settlement and inclination of the Prasat Suor Prat N1 Tower as mentioned in Table 2.19.

Figure 2.38 shows the distribution of the displacement of the tower for Case A and Case B. From the figure it is obvious that the tower in both cases were tend to incline to the North (N) rather than to the South (S), but Case B experienced higher settlemet than Case A. This higher settlement was the effect of

the loosen compaction of the rammed earth and the self-weight of the tower itself. Furthermore, the different settlement between the North and South cause the tower experiences inclination for both cases. The color legend shows the displacement of the masonry blocks in meter. Tower in Case A had smaller displacement compare to Case B because the settlement cause the blocks' movement. The maximum displacement occurred in Case A was around 0.9-1.0 m on the North section. While for Case B, in the same section, it had displacement around 1.0 -1.17 m. The displacement in the North section was higher than the South section due to different settlement in each section.

Table 2.19 Settlement and Iclination of the Prasat Suor Prat N1 Tower (Hashimoto et al., 2014)

Case	Settlement (m)	Inclination (%)
A	0.165	2.36
B	0.195	2.76

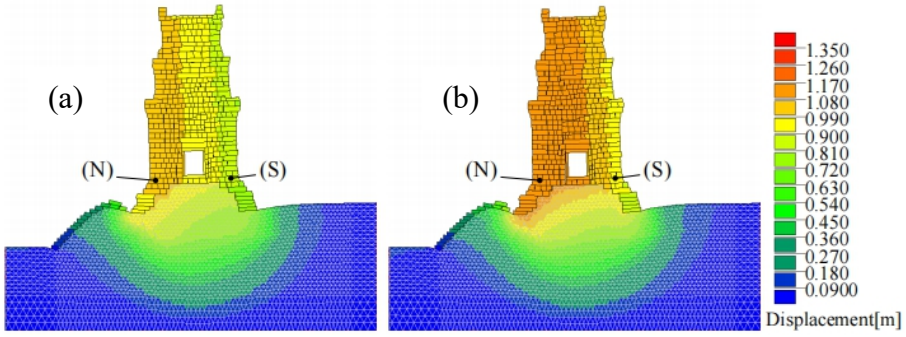

Figure 2.38 Distribution of the displacement of the tower, (a) Case A, and (b) Case B (Hashimoto et al., 2014).

Research by (Kamai et al., 2005) is adopting the DDA for back analysis of historical masonry structures in Israel. Two historical masonry structure were

choosen to become the object of the research, namely Avdat and Mamshit. To obtain the mechanical properties of the blocks of the masonry structure, laboratory tests were conducted by taking the blocks specimen from two site and testing it in laboratory. The obtained data of the material properties is mentioned in Table 2.20.

Mamshit initially was an ancient church which some parts already collapse. Figure 2.39 shows the real condition of the Mamshit where most of the masonry blocks already collapse. The entrance which depicted as an arch or the key stone shows displacement by sliding downwards from its arrangement up to 4 cm (Kamai et al., 2005). The main difficulties in modelling the masonry structure, especially the arch was the heterogencity of the blocks. The blocks came in different shape and size. Besides, some of the blocks already collapse, hence the modelling need to be conducted closely in order to match with the failure pattern on observation site. But, using DDA, this difficulties can be overcome. The geomtery of the Mamshit generated using DDA is shown in Figure 2.40.

Table 2.20 Mechanical properties for the Avdat and Mamshit (Kamai et al., 2005)

Mechanical property	**Avdat**
Density (Kg/m^3)	2555
Porosity (%)	5
Dynamic Young's modulus (GPa)	54.2
Dynamic Poisson's ration	0.33
Dynamic Shear modulus (GPa)	20.3
Interface friction angle	35

Figure 2.39 Real condition of Mamshit in Israel (Kamai et al., 2005)

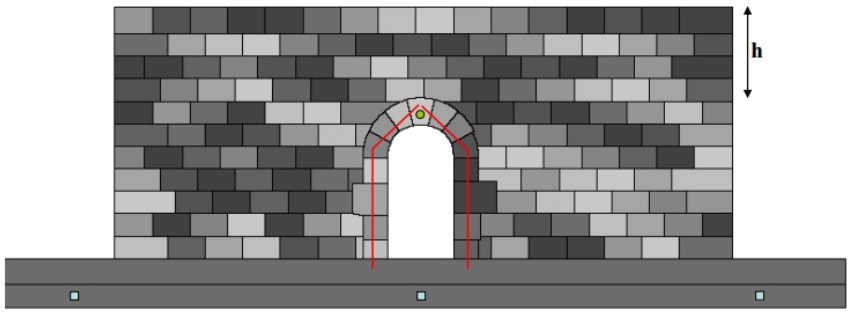

Figure 2.40 Geometry of Mamshit using DDA (Kamai et al., 2005)

The analysis using DDA is conducted under two loading mechanism where the foundation imposed with time dependant displacement (this loading called ‘dis mode’), while the second mechanism is called ‘qk mode’ where all centroid of the blocks imposed to time dependant acceleration (Kamai et al., 2005). For the ‘dis mode’ the key stone in the arch undergo displacement to upward direction and all blocks are deformed. While in the ‘qk mode’ the keystone occur small displacement in downward direction and the other blocks

not experiencing displacement. The derfomation due to loading mechanism is depicted in Figure 2.41.

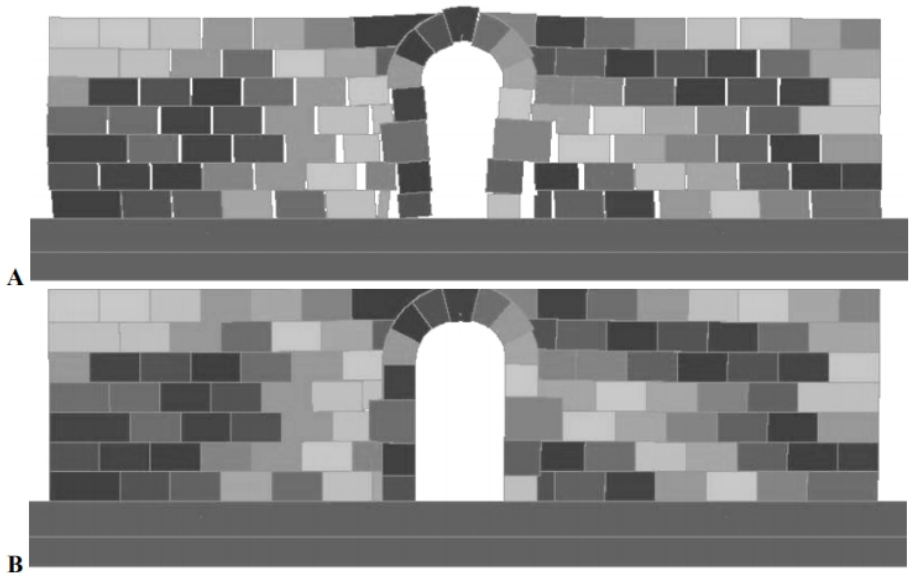

Figure 2.41 Deformation of Mamshit due to (a) 'dis mode', (b) 'qk mode' (Kamai et al., 2005)

The last research in DDA is condected by (Ma et al., 1996) for analysing the mosca bridge under earthquake load. This bridge is located in Turin, Italy and made of Malanggio granite. The span is 45 m length and the rising of the intrados is 1.5 m. The detailed geometry of the bridge generated by DDA is depicted in Figure 2.42, where the voussoir is consist of 93 blocks. Each block in the voussoir is modelled by a single element in DDA. Blocks that become the observation point are symbolized as block 1 until 5.

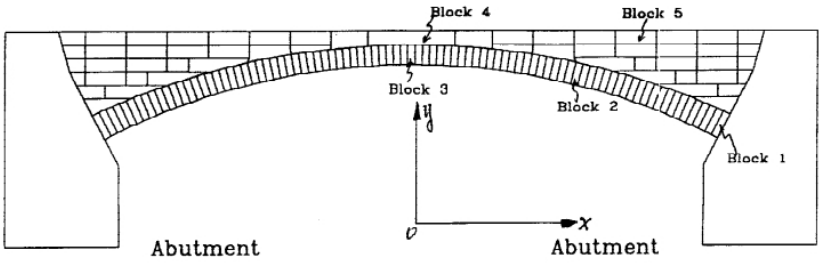

Figure 2.42 Geometry of the Mosca bridge using DDA (Ma et al., 1996)

The mechnanical properties of the block are define as Young's modulus of 4.5 GPa and the unit weight is 2.4 tons/m^3, while the mechanical properties of joint, the normal stiffness is 4.5 GPa (Ma et al., 1996). For the earthquake load, the frequanecy applied is 2.5 and sinusoidal acceleration is 0.5g. Since comercial computer software is not available in DDA, (Ma et al., 1996) was using a software generated individually by the author.

The result of the analysis usind DDA is depicted in Figure 2.43. that shows the principle stresses distribution at the end of the loading which is at 0.42 second (Ma et al., 1996). From Figure 2.43, it is obvious that higher stresses is concentrated at the mid span of the bridge. It is possible to happen since the cross section in the mid span is narrower than other section. Although the overall structure is stable and there are not collapse occur, only displacement of the blocks. It also important to be noted that block 3 and block 4 at the mid span experience higher horizontal stresses in phase but different magnitude. (Ma et al., 1996).

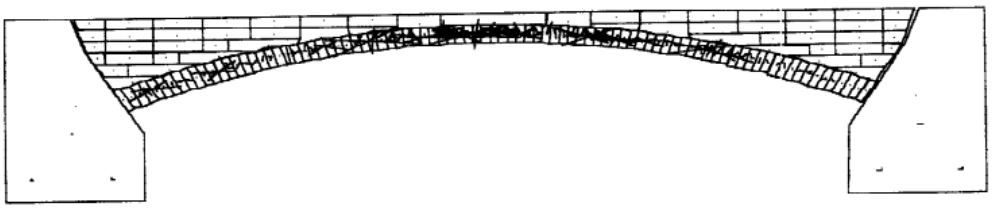

Figure 2.43 Result of analysis using DDA (Ma et al., 1996)

2.3 Mortar Joint Properties

In this section, the prelimenary studies about the joint' properties affecting the shear stress of the masonry structure are explained. As mention in the previous chapter, there are several mortar joint properties of the masonry structure such as Joint Roughness, Joint Compressive Strength, Joint Friction, Joint Cohession, and Joint Tensile. Among those properties, prelimenary studies already conducted to investigate which are the paramount properties of the joint that govern the failure mechanism at the joint. The authors and their researches along with the focused of the joint properties investigate are tabulated in Table 2.21 and Table 2.22, respectively.

Table 2.21 Authors and Papers Discussing the Joint's Parameters affecting the Shear Stress of the Masonry Structure

Number	Author	Paper
(1)	Idris et al. (2009) (Idris et al., 2009)	Numerical Modelling of Masonry Joints Degradation in Built Tunnels
(2)	Rahman and Ueda (2014)	Experimental Investigation and Numerical Modeling of Peak Shear Stress of Brick Masonry

	(Rahman & Ueda, 2014)	Mortar Joint Under Compression
(3)	Sarhosis et al. (2015) (Sarhosis et al., 2015)	Influence of Brick-Mortar Interface on the Mechanical Behaviour of Low Bond Strength Masonry Brickwork Lintels
(4)	Hossain et al. (2016) (Hossain et al., 2016)	Friction on Mortar-less Joints in Semi Interlocking Masonry

Table 2.22 Joint Properties that become the main focused of the research by another authors

Number	Author	Joint Cohession	Joint Tensile Strength	Joint Friction Angle
(1)	Idris et al. (2009)	√	√	√
(2)	Rahman and Ueda (2014)	√		√
(3)	Sarhosis et al. (2015)	√	√	√
(4)	Hossain et al. (2016)			√

(Idris et al., 2009) on his research stated that the constituent of the mortar joint generally made of lime of cement mortar. By using DEM (Distinct Element Method), (Idris et al., 2009) focussed on the evolution of the joint properties and its effect on the strength of masonry structure. The analysis was done using the UDEC (Universal Distinct Element Code) by Itasca. The masonry behaviour

globally observes through response of two types of joint. Those are Total Length of Open Joint (TLOJ) and Total Length of Joint at Limiting Friction (TLJLF).

Two types of joint mentioned previously was influenced by joint properties. (Idris et al., 2009) suggested of using Joint Cohession (jcoh), Joint Friction Angle (jfric), and joint Tensile Strength (jtens) as an independent variables. Hence, (Idris et al., 2009) was using 27 speciemen as a test number to investigate the influence the evolution of those joint properties to masonry behaviour. The value of each joint properties were defined for each specimen. The joint cohession values ranging from 0.2 – 0.8 MPa, while for the joint tensile strength the values ranging from 0.25 – 0.75 MPa. To add more, for the joint friction the values ranging from 5^0 – 15^0. The detail distribution for value of each parameter and specimen are listed in Table 2.23.

The object of the reseach was masonry arch of an underground tunnels which consists of blocks attached with mortar joint. The surrounding of the arch consists of homogenous soil consists of mixture of sand and clay. The element of the blocks are square and rectangular blocks. The curvature of the arch was 80 cm width and the thickness of each element block was 20 cm. The constituent of the mortar joints were made by lime mortar. And it was assumed that the masonry arch model was symetry, hence detail dimension and geometry of the masonry arch is decribe in Figure 2.44.

Table 2.23 Distribution of Value for each joint properties and specimen (Idris et al., 2009)

Specimen number	Joint Cohession (MPa)	Joint Tensile Strength (MPa)	Joint Friction Angle (^{0})
1	0.8	0.75	25
2	0.8	0.75	15
3	0.8	0.75	5
4	0.8	0.5	25
5	0.8	0.5	15
6	0.8	0.5	5
7	0.8	0.25	25
8	0.8	0.25	15
9	0.8	0.25	5
10	0.5	0.75	25
11	0.5	0.75	15
12	0.5	0.75	5
13	0.5	0.5	25
14	0.5	0.5	15
15	0.5	0.5	5
16	0.5	0.25	25
17	0.5	0.25	15
18	0.5	0.25	5
19	0.2	0.75	25
20	0.2	0.75	15
21	0.2	0.75	5
22	0.2	0.5	25
23	0.2	0.5	15
24	0.2	0.5	5
25	0.2	0.25	25
26	0.2	0.25	15
27	0.2	0.25	5

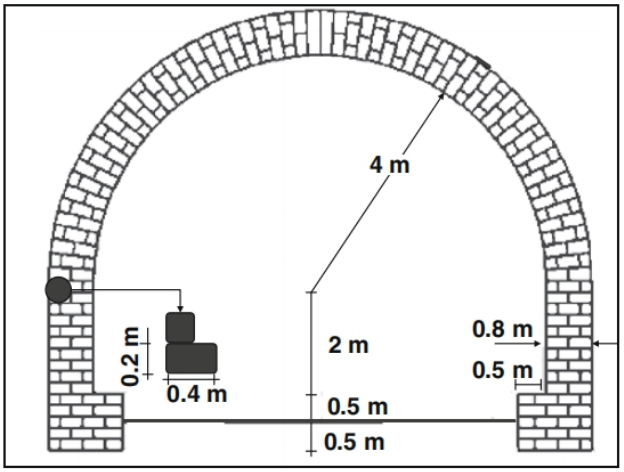

Figure 2.44 Masonry arch structure generated using DEM (Idris et al., 2009)

The influence of each joint properties were rather difficulty to distinguished, therefore (Idris et al., 2009) suggested to adopt the 3D responnse surface analysis to investigate the influence of each joint properties accurately. Multiple linear regression analysis also proposed by (Idris et al., 2009) on this research as supporting evidence of the prelimenary analysis. Pedhazur (1997) on research by (Idris et al., 2009) stated that multiple linear regression analysis is important to provide relationship between the dependent variables and the independent variables. In this research, the dependent variables are the Total Length of Open Joint (TLOJ) and Total Length of Joint at Limiting Friction (TLJLF), while the independent variables are Joint Cohession (jcoh), Joint Friction Angle (jfric), and joint Tensile Strength (jtens).

The result of the analysis of using variance value of joint properties for the TLOJ and TLJLF is depicted in Figure 2.45 and Figure 2.46, respectively. The black dots are the respond that observed due to joint cohesion, friction, and tensile strength.

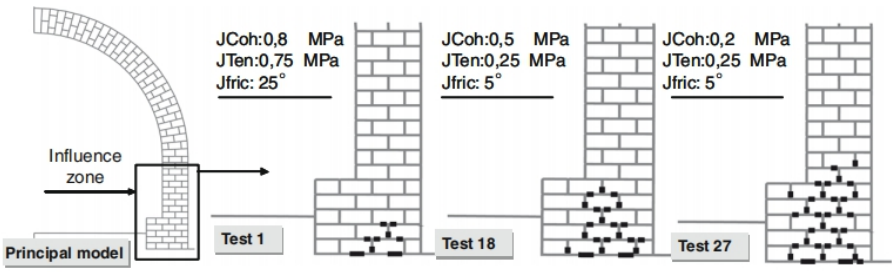

Figure 2.45 The sample of the analysis for the Total Length of Open Joint (TLOJ) (Idris et al., 2009)

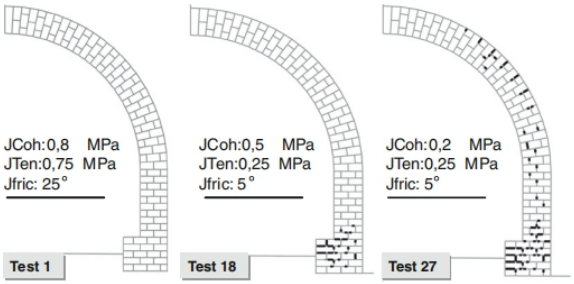

Figure 2.46 The sample of the analysis for the Total Length of Joint at Limiting Friction (TLJLF)
(Idris et al., 2009)

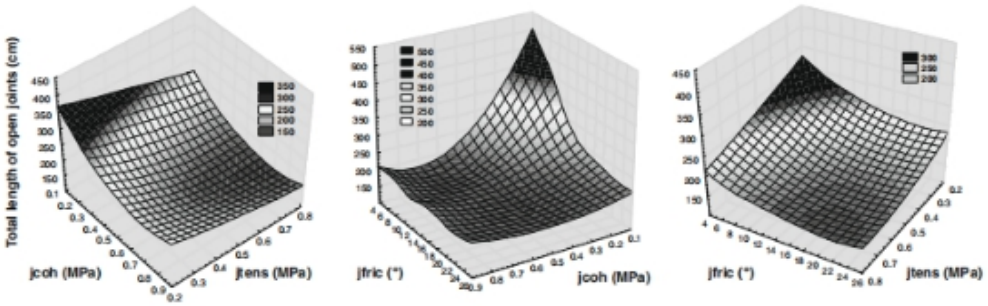

Figure 2.47 Respons of the Joint Properties towards the Total Length of Open Joint (TLOJ) (Idris et al., 2009)

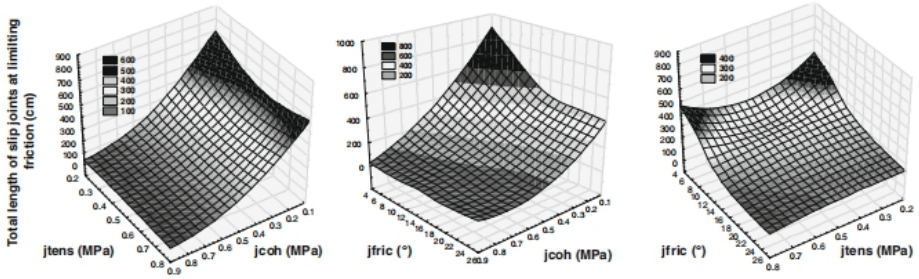

Figure 2.48 Respons of the Joint Properties towards the Total Length of Joint at Limiting Friction (TLJLF) (Idris et al., 2009)

Based on 3D response surface analysis, major findings related to joint properties are discussed. To describe the influence of the joint properties on TLOJ and TLJLF, the result is depicted in Figure 2.47 and Figure 2.48, respectively. Turn out, joint cohesion is having the substantial influence in TLOJ. To add more, the combination of the joint cohesion and joint friction angle generate the highest total length of the TLOJ compare to other combination as seen in Figure 2.47, where the degradation of the joint cohesion and friction angle cause the total length of the TLOJ increasing. Same as TLOJ, the joint properties that control the total length of TLJLF are joint cohesion and joint friction as describe in Figure 2.48. While for the joint tensile sterngth, it influence the total length of both joint but insignificant.

Multiple linear regression model also adopted to strengthen the result of the analysis. In this analysis, the joint properties are ranked according to its influence to joint. The first rank for the TLOJ is the joint cohesion followed by the joint tensile strength and joint friction angle, but the combination of joint cohesion and joint friction angle is the most significant properties that influence the TLOJ (Idris et al., 2009). On the other hand, the joint cohesion and joint friction angle are the governing joint properties towards the TLJLF.

Another research by (Rahman & Ueda, 2014) study about the affecting factors of the shear stress and displacement on bed joints for masonry structure. The experimental test was conducted by using wire-cut clay brick with four different types of mortars, namely E, M, S, and N. The dimension of the bricks were 250 mm length, 120 mm wide, and 170 mm thick and the bricks were

soaked in water before arranged with the mortar with the degree of saturation was controlled to be 80% (Rahman & Ueda, 2014). While the detailed specification for the specimen using different mortar is decribed in Table 2.24. The specimen and the instrumen for triplet shear test is depicted in Figure 2.49.

Table 2.24 Specification of the specimen using different mortar (Rahman & Ueda, 2014)

Mortar Type	Cement:sand (by volume)	Water/cement (by weight)	Compressive strength (MPa)	Splitting tensile strength (Mpa)	Young's Modulus (GPa)	Poisson's ratio (ν)	Flow
E	1:2.25	0.50	28.5	3.0	26.0	0.186	170
M	1:2.75	0.70	20.0	1.7	19.3	0.156	212
S	1:3.5	0.86	12.5	1.5	15.7	0.200	221
N	1:4.0	0.95	10.0	0.9	14.5	0.188	190

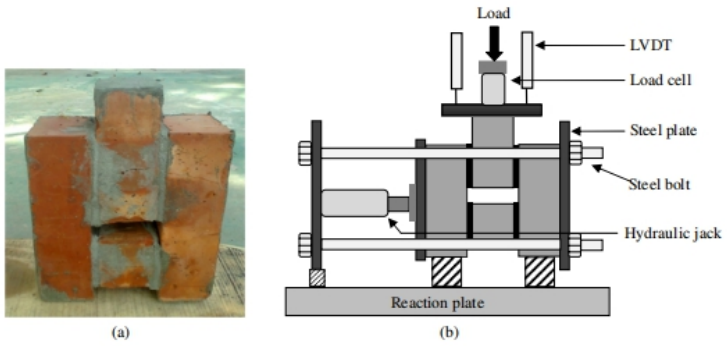

Figure 2.49 Specimen and equipment for triplet shear test (Rahman & Ueda, 2014)

Two important parameters are focused in this study, those are the confining pressure and mortar strength, which noticed as major factors

contributing to the shear capacity at the brick-mortar interface. The result of the experimental test shows that the influencing factor of the shear strength is not only the confining pressure, but also the characteristics of bond between mortar and brick (cohesion) and coefficient of friction between the two sliding surface (friction) (Rahman & Ueda, 2014).

Figure 2.50 shows the result of the experimental test of normal stress towards the shear strength and residual strength. In Figure 2.50(a), the peak shear stress governed by the strength of the mortar. Unlike friction angle (Ø) which is dependant on normal stress, the cohesion (c) is independent of normal stress, hence small increment occurs respect to increasing of mortar strength. While for case in Figure 2.50(b), the ratio between the residual friction coefficient towards residual shear strength is increase constantly at the time when the cohesion is lost.

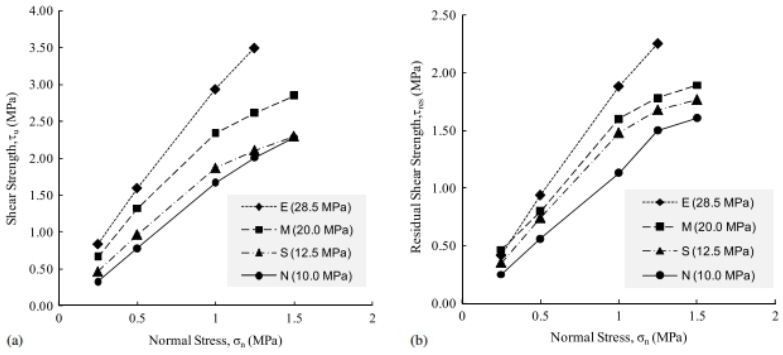

Figure 2.50 Effect of normal stress towards, (a) shear strength, (b) residual shear strength (Rahman & Ueda, 2014)

(Sarhosis et al., 2015) also conducted a research about the the influence of joint properties on the mechanical behaviour of masonry structure. In this research the masonry stucture was lintel or threshold of the door which made of bricks.

Numerical test along with experimental test were used to simulate the behaviour of the lintel where it was assume to have low bond of joints. DEM (Distinct Element Method) was choosen to model the masonry structure and UDEC (Universal Distinct Eleement Code) was adopted to as the numerical program.

The value of material properties which include the elastic parameters, interface joint parameters, and inelastic parameters, are mentioned in Table 2.25. The value for the material properties were obtained from several studies previously by another authors, then by using ANOVA (Analysis of Variances) to identify the relative value of those parameters (Sarhosis et al., 2015). The analysis were conducted until two loading conditions were satisfied, namely, the loading until the first crack and when the ultimate load was reached.

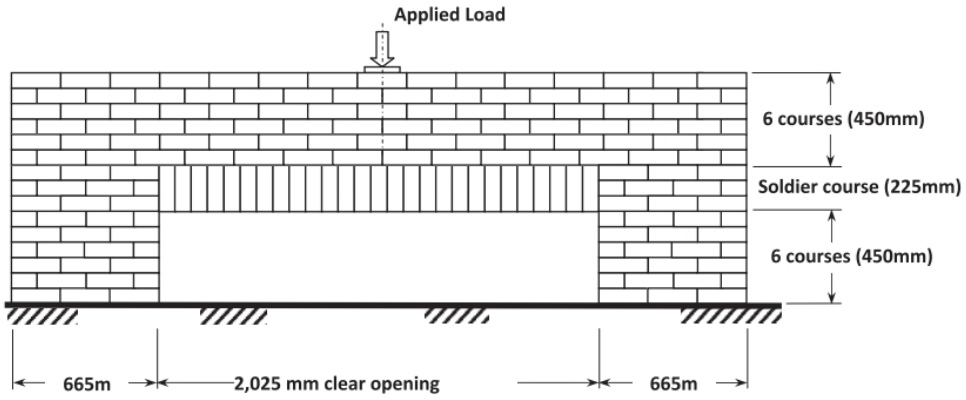

Figure 2.51 Dimension and profile of the masonry lintel (Sarhosis et al., 2015)

For the first loading condition, the inelastic parameters of mortar joints such as Joint Cohession (jcoh), Joint Friction Angle (jfric), and Joint Tensile Strength (jtens), were influencing the most. While for the second loading

condition, the elastic parameters such as Joint normal stiffness (JKn) and joint shear stiffness (JKs) define the most (Sarhosis et al., 2015).

The numerical tests were conducted by 125 experiments where the value of Joint Cohession (jcoh), Joint Friction Angle (jfric), Joint Tensile Strength (jtens), Joint normal stiffness (JKn), and joint shear stiffness (JKs) were vary. Those properties become the independent variables that defines the overall strength of the masonry lintel. The dimension and profile of the masonry lintel is decribe in Figure 2.51.

Table 2.25 Material properties of the Blocks and Joints (Sarhosis et al., 2015)

Unit parameters	**Symbol**	**Value**	**Units**
Elastic parameters			
Density	d	2000	Kg/m^2
Elastic modulus	E	6050	MPa
Poisson's ratio	V	0.14	-
Interface joint parameters			
Joint normal stiffness	JKn	50-90	GPa/m
Joint shear stiffness	JKs	30-85	GPa/m
Inelastic parameters			
Joint friction angle	^{0}	20-40	Degrees
Joint cohesion	Jcoh	0.05-0.15	MPa
Joint tensile strength	Jten	0.05-0.15	MPa
Joint dilatation angle		0	Degrees

The result of the test at the first crack and ultimate load in Figure 2.52 and Figure 2.53, respectively. In the Figure 2.52(a), the increasing of the directly proportional to the first cracking in the masonry. The relationship is depicted in

linear line. Hence, joint tensile strength is the predominant factor that influence the occurring of the first crack. On the other hand, the joint friction angle and joint cohesion do not have significant influence towards the first crack as depicted in Figure 2.52(b) and Figure 2.52(c) (Sarhosis et al., 2015).

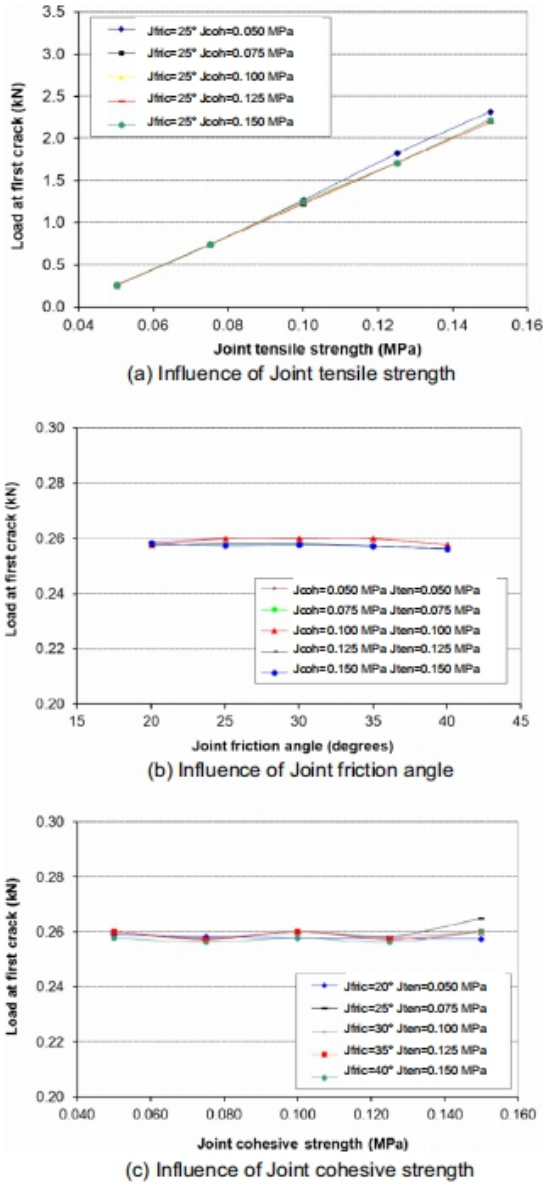

Figure 2.52 Influence of joint parameters at first crack (Sarhosis et al., 2015)

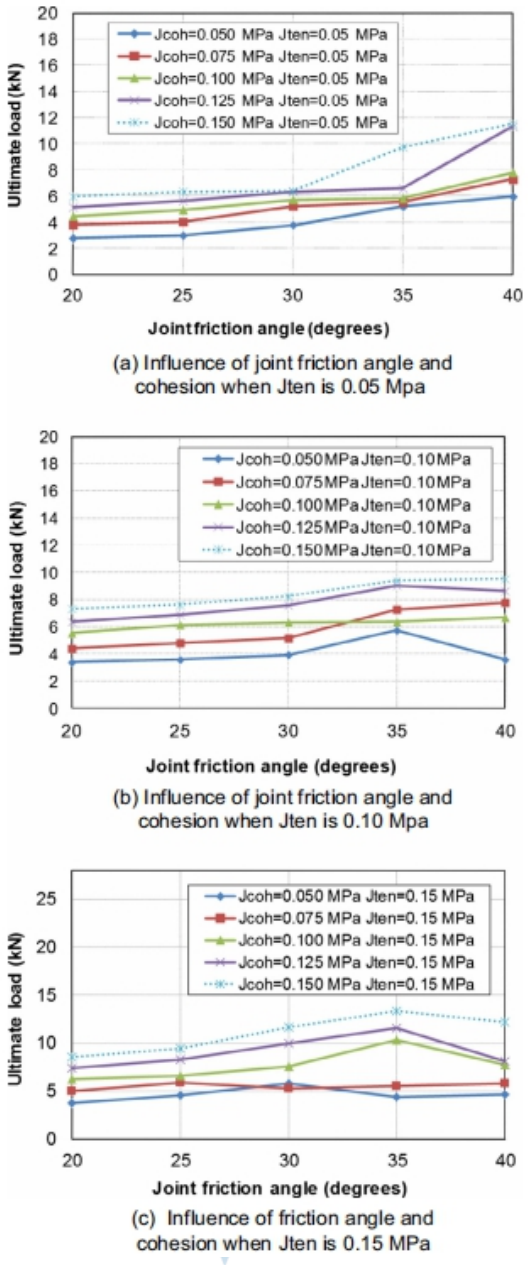

Figure 2.53 Influence of joint parameters at ultimate load (Sarhosis et al., 2015)

In Figure 2.53 the graph depicted is more focus on the influence of joint friction and joint cohesion when joint tensile strength assumes in several value. In Figure 2.53(a), the joint tensile strength is set to be constant at 0.05 MPa, while the joint friction and cohesion vary. While for the Figure 2.53(b) and Figure

2.53(c), the joint tensile strength is set to be constant at 0.10 MPa and 0.15 MPa, respectively. The result shows that the joint friction angle influences the increasing of the capacity of the ultimate load when the value ranging from 20^0 to 30^0. While when the internal friction angle is 30^0 to 40^0, the influence of the friction angle become not proportional.

Hence, (Sarhosis et al., 2015) proposed that the threshold value of joint friction is 30^0. Because when the value ranging from 20^0 to 30^0 the capacity of the ultimate load increase rapidly, conversely, the joint friction angle does not fully impact and increase the capacity of ultimate load when the value is 30^0 to 40^0. The sequence of important joint properties according to (Sarhosis et al., 2015) is 1) joint cohesion, 2) joint friction angle, and 3) joint tensile strength, and the combination of joint cohesion and friction shows noteworthy impact towards the mechanical response to failure

On the other hand, (Hossain et al., 2016) on his research only focused on friction of the mortar-less joint or interface of the blocks for SIM (Semi Interlocking Masonry). The experimental test, namely couplet shear test was conducted to obtain the coefficient of the friction of the SIM blcoks when the loading was placed. Two loading condition were considered in the research, which are dynamic and cyclic loading. The shape and dimension of the SIM block is depicted in Figure 2.54. The compressive strength of the SIM block was 33.75 MPa, while the density was 2350 kg/m^3. Vasconcelos and Lourenco (2009a) on paper by (Hossain et al., 2016) suggested that the cohesion of dry masonry

joint can be assumed equal to zero, hence the Mohr-Coulomb failure criterion can be linear as depicted in Figure 2.55.

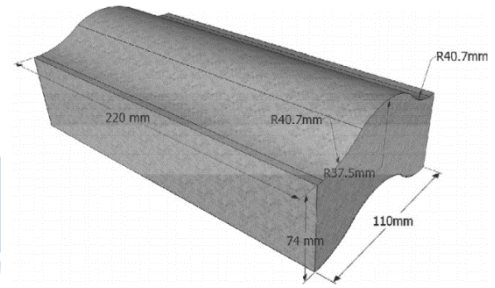

Figure 2.54 Shape and Dimension of the specimen (Hossain et al., 2016)

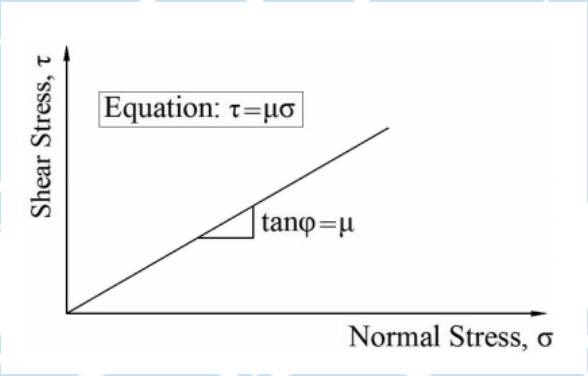

Figure 2.55 Suggested Mohr-Coulomb failure criterion for dry joint masonry (Hossain et al., 2016)

The blocks surface were prepared into three conditons. First the surface was fully dry or can be called as dry surface, the second condition was the surface greased with linssed oil made of putty, and the third condition was the surface attached with rubber foam tape (Hossain et al., 2016). The prescribed loads for the pre-compression were setted for 800 N and 1600 N, where the load was assigned in vertical axis. For the experimental test, each unit listed in Table 2.26 was made into three testing specimens. Therefore, in total there are 36 testing specimens for

this research. The surface treatment along with the loading condition of each specimen is decribe in Table 2.26.

Table 2.26 Treatment for testing the SIM blocks (Hossain et al., 2016)

Unit Name	Type of Loading	Surface Treatment	Pre-compression Load (N)
TBM-D	Dynamic	Dry Surfaces	800
TBB-D	Dynamic	Dry Surfaces	1600
TPM-D	Dynamic	Surfaces with putty	800
TPB-D	Dynamic	Surfaces with putty	1600
TTM-D	Dynamic	Surfaces with tape	800
TTB-D	Dynamic	Surfaces with tape	1600
TBM-S	Static	Dry Surfaces	800
TBB-S	Static	Dry Surfaces	1600
TPM-S	Static	Surfaces with putty	800
TPB-S	Static	Surfaces with putty	1600
TTM-S	Static	Surfaces with tape	800
TTB-S	Static	Surfaces with tape	1600

From the experimental test result, (Hossain et al., 2016) stated that paramount parameter of the SIM is the coefficcient of friction since it is able to dissipate energy dueing the earthquake. Different treatment of the SIM surface also become important factors that inluence the friction of the SIM units. The result of different treatment of the SIM surface in dynamic and statis test is depicted in Figure 2.56.

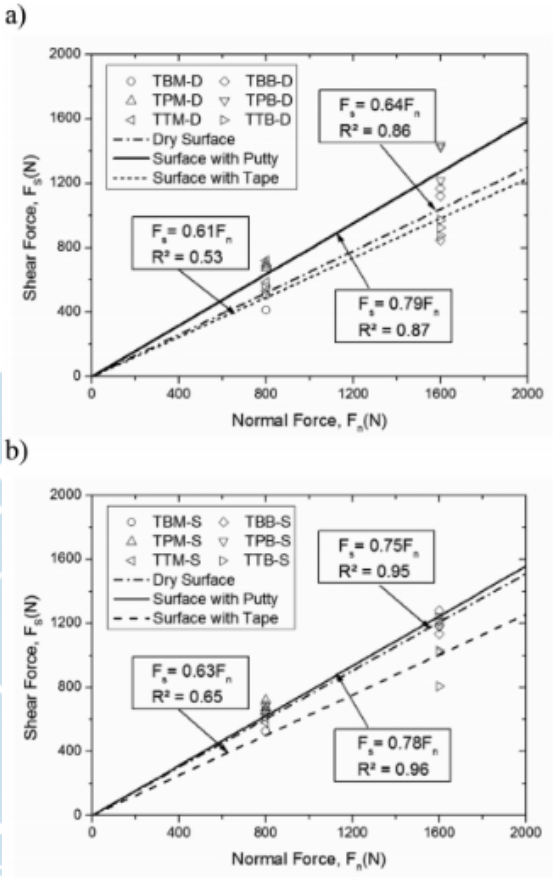

Figure 2.56 Mohr Coulomb failure criterion, (a) dynamic test and (b) static test (Hossain et al., 2016)

From the result of both dynamic and static test in Figure 2.56, the surface applied with putty has the highest coefficient of friction compares to another surface treatment. According to (Hossain et al., 2016), the surface with highest coefficent of friction, in case the surface with putty, can dissipate higher seismic energy, hence the masonry structure can be more stable.